Advances in remote/aerial sensing techniques for monitoring soil health

Jeffrey P. Walker and Nan Ye, Monash University, Australia; and Liujun Zhu, Monash University, Australia and Yangtze Institute for Conservation and Development, Hohai University, China

1 Introduction

Due to its dependencies on weather, topography, land surface type, and texture, the status of soil varies significantly in time and space. Although conventional ground monitoring stations have been widely used to capture the temporal variation of environment parameters at point-based scales, their applications are limited by poor spatial representativeness, high cost of installation and maintenance, and interference with farming activities. Remote sensing provides a cost-effective alternative for soil health monitoring. In principle, sensors are mounted on a remote sensing platform, such as satellite, aircraft, drone or vehicle, and subsequently used to measure the energy from the soil surface. The properties of the received signals can be linked to soil-related parameters (e.g. soil moisture, roughness, salinity) within the field of view through physical and/or empirical models. Compared with in situ approaches, remote sensing techniques have the desired capability of providing spatially explicit maps of soil parameters, with up to global coverage. Several remote sensing techniques (e.g. optical, microwave, nuclear, and gravity) have been developed for monitoring the land surface conditions. However, due to its

http://dx.doi.org/10.19103/AS.2022.0107.05

all-weather capability and ability to penetrate the vegetation layer, even into the soil itself, microwave remote sensing has become widely acknowledged as a key technique for the agricultural industry.

Microwave remote sensing measures the electromagnetic radiation in the microwave spectrum, ranging from 0.3 GHz to 40 GHz. This spectrum region is further divided into eight bands as listed in Table 1. By measuring intensity, polarization, phase, and/or other properties of microwave radiation, the dielectric and/or geometric properties of the sensed target can be detected. For soil material, the dielectric constant varies with soil water content from approximately 3.5 for very dry soil to approximately 40 for saturated soil (Ulaby et al., 1986), forming the fundamental basis of microwave remote sensing for soil moisture content. The relationship between soil dielectric constant and soil moisture is shown in Fig. 1, with both real and imaginary parts of the soil dielectric constant increasing with soil water content, and the relationship influenced by soil particle size distribution (Ulaby et al., 1986).

A dielectric constant is a complex number ($\varepsilon' - j \cdot \varepsilon''$), where $j = \sqrt{-1}$, with the real (ε') and imaginary (ε'') parts determining the propagation speed of the electromagnetic wave through the soil medium and the loss of electromagnetic energy, respectively. Normally, it is expressed as a relative value which is the ratio of the dielectric constant of material to that of free space. Due to the three phases of soil, soil dielectric constant is a combination of the individual constituents including soil particles, water, and air components. The value of soil dielectric is also affected by other factors, including soil texture, temperature, salinity, and electromagnetic wavelength. To relate soil dielectric constant to volumetric soil moisture, several semi-empirical mixing models have been developed to estimate soil dielectric constant from the knowledge on electromagnetic wavelength, soil texture, bulk density, and salinity (Dobson et al., 1985; Hallikainen et al., 1985; Mironov et al., 2004; Wang and Schmugge, 1980). In these, the dielectric constant of moist soil was found to be slightly dependent on temperature, and so under most natural temperature conditions,

Table 1 Microwave band designations

Band designation	Wavelength (cm)	Frequency (GHz)
P	100.0–30.0	0.3–1.0
L	30.0–15.0	1.0–2.0
S	15.0–7.50	2.0–4.0
C	7.50–3.75	4.0–8.0
X	3.75–2.40	8.0–12.5
K_u	2.40–1.67	12.5–18.0
K	1.67–1.10	18.0–26.5
K_a	1.10–0.75	26.5–40.0

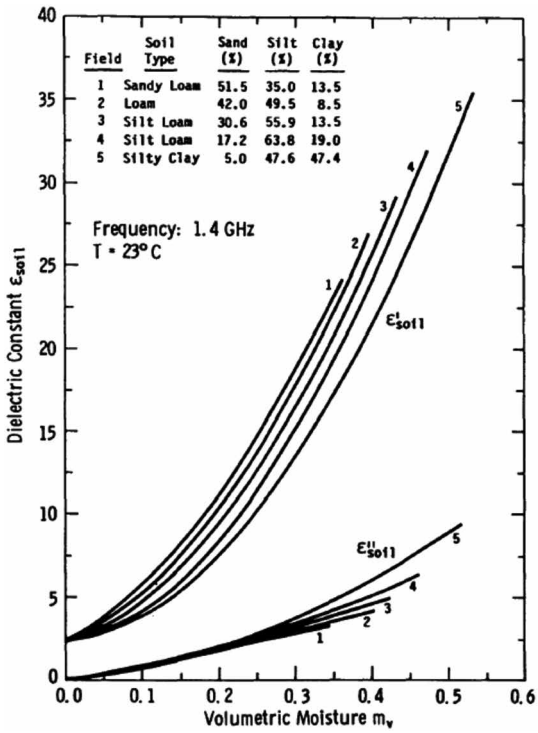

Figure 1 Soil dielectric constant as a function of volumetric soil moisture for five soils at 1.4 GHz. Smooth curves were drawn through measured data points. Source: Ulaby et al., (1986).

the effect of temperature on soil dielectric constant can be ignored. However, when soil gets frozen, its dielectric constant is reduced significantly since the dielectric constant of the water constituent changes from that of liquid water (approximately 80) to that of ice (approximately 3).

Based on the provision of electromagnetic radiation sources, microwave remote sensing techniques are divided into two categories: active and passive. Active microwave remote sensing instruments, known as radars, transmit a pulse of microwave radiation and measure the signal scattered back in the direction of the sensor. The coefficient between the power of the transmitted and received signal is dependent on the reflectivity of the target, which in soil material is related to the soil moisture content. In contrast, passive remote sensing instruments, referred to as radiometers, do not transmit any electromagnetic waves but only receive the self-emitted radiation from the land surface at a specific microwave frequency. The intensity of microwave emission of soil relies mainly on soil temperature and soil surface emissivity, which in turn correlates with soil moisture content through the soil dielectric constant.

The following subsections provide a general description of the principles and features of active and passive microwave remote sensing of soil moisture.

2 Active microwave remote sensing

Active microwave remote sensing has been widely used to map soil moisture at regional to global scales. The radar system generally consists of a transmitter, receiver, antenna, and processer. An electromagnetic pulse in the microwave frequencies is generated in the transmitter and transmitted to the target through the radar antenna. Over land surfaces, a part of the transmitted electromagnetic wave is scattered by the vegetation canopy and/or soil surface, and returned back to the radar system. The backscatter signal is collected by the same antenna and its intensity is measured by the receiver. The coefficient between the power of the transmitted and backscattered signal is obtained in the processer, which can be related to the water content of the sensed soil target. The most common active microwave mapping configuration is the synthetic aperture radar (SAR), which can provide a spatial resolution in the order of tens of meters over a swath of 50–500 km. Currently, five space-borne SAR systems are operating at microwave frequencies for soil moisture observations: European Space Agency (ESA)'s ERS-1/2 C-band SAR, ESA's ENVISAT (ERS-3) C-band ASAR (Advanced SAR), the Canadian C-band RADARSAR-1/2, the Japanese L-band ALOS (Advanced Land Observing Satellite) PALSAR (Phased Array type L-band SAR), and the German X-band TerraSAR.

The electromagnetic waves sent and received by radars are normally polarized either horizontally (H) or vertically (V), and therefore there can have four polarization combinations: HH, VV, HV, and VH, where the first and second letters represent the polarization of transmitted and received signals, respectively. The backscattering coefficient σ_{pp} in decibels [dB] at the polarization of p is used to describe the intensity of the backscattered radiation (Ulaby et al., 1982). For a given target, the backscattering coefficient is dependent on wave polarization, frequency, and incidence angle (Ulaby et al., 1982). Under bare soil conditions, the backscattering coefficient obtained using a radar system operating at consistent polarization, frequency, and incidence angle is affected by the dielectric constant of the soil and surface roughness (Ulaby et al., 1986). Under vegetated soil conditions, the backscattering coefficient is dependent also on the attenuation effect of the vegetation layer which makes the backscattering response more complicated (Ulaby et al., 1982). In addition, since the soil moisture retrieval is normally based on a flat land surface assumption, the topographic relief causes a variation of local incidence angle and significantly affects the backscattered signal (Van Zyl et al., 1993).

The total co-polarized backscatter σ_{pp}^{T} from the land surface is the sum of three components, given as:

$$\sigma_{pp}^{T} = \sigma_{pp}^{vol} + \sigma_{pp}^{S} \cdot \exp\left(-2 \cdot \tau_{C}\right) + \sigma_{pp}^{int}, \quad (1)$$

where the first term is the backscatter from the vegetation volume σ_{pp}^{vol}, and the second term is the soil surface backscatter σ_{pp}^{S} attenuated by a vegetation layer with opacity of $\tau_C$during both transmitting toward and reflecting from the soil surface. The third term σ_{pp}^{int} is the interaction between the vegetation and soil surface (Ulaby et al., 1996). For bare or low vegetated soils, the total backscattering coefficients σ_{pp}^{T} is dominated by σ_{pp}^{S} and thus dependent mainly on the soil moisture and surface roughness, while for highly vegetated soil, the σ_{pp}^{T} is determined primarily on the volumetric scattering from the vegetation canopy σ_{pp}^{vol}. Numerous theoretical, empirical, and semi-empirical models have been developed to retrieve the soil electric constant and subsequent soil moisture content from radar backscattering data (Dubois et al., 1995; Fung et al., 1992; Oh et al., 1992; Shi et al., 1995) (Fig. 2).

2.1 Theoretical approaches

Theoretical approaches have been developed based on the diffraction theory of electromagnetic waves to describe the microwave backscattering from land surfaces with known roughness characteristics. Their applicability is limited to the frequency of electromagnetic waves and the range of surface roughness (D'urso and Minacapilli, 2006; Fung et al., 1992).

Most of the currently used surface scattering models have been derived from the small perturbation model (Rice, 1951) and Kirchhoff model (Beckmann and Spizzichino, 1963), which are restricted to slightly rough surfaces and very rough surfaces, respectively. The integral equation model (IEM) (Fung, 1994b; Fung et al., 1992) combines these two theories and is thus applicable to a wider

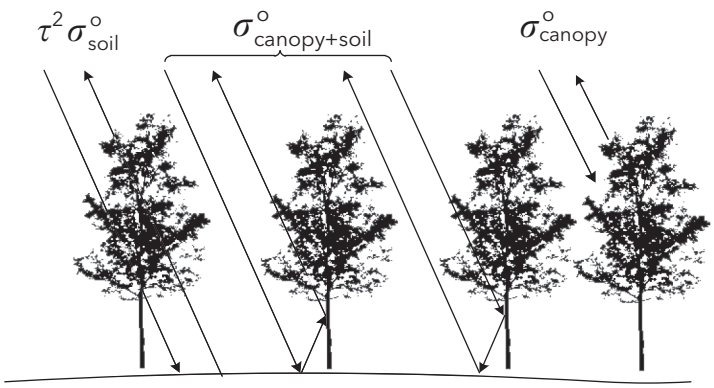

Figure 2 Backscattering mechanics of vegetated soil. Source: modified from Ulaby et al. (2014).

range of roughness conditions than conventional models, such as the physical optical model and geometric optical mode (Fung, 1994b; Shi et al., 2005).

Although the theoretical models can predict the general variation of backscattering coefficient in response to changes in roughness and soil moisture content (Dubois and Van Zyl, 1994), their complexity and the restrictive requirement for the parameterization of the vegetation and soil surface layer limits their effective applicability for the soil moisture retrieval (Ulaby et al., 1986).

2.2 Empirical approaches

Being limited by their validity regions, theoretical backscattering models are not valid for many natural land surface conditions. In addition, theoretical models fail to estimate backscatter in good agreement with experimental radar backscatter measurements (Oh et al., 1992; Walker et al., 2004). Therefore, many empirical models have been developed from experimental measurements to establish the relationship between soil moisture and backscattering observations (Walker et al., 2004).

The most commonly used empirical method is a linear assumption between soil moisture and radar backscattering polarization index. For example, Shoshany et al. (2000) proposed an empirical soil moisture retrieval method using the normalized backscatter moisture index (NBMI) which is defined as:

$$\mathrm{NBMI} = \frac{\sigma_{t1} - \sigma_{t2}}{\sigma_{t1} + \sigma_{t2}}, \tag{2}$$

where σ_{t1} and σ_{t2} are the backscatter coefficients at different time steps. Subsequently, the volumetric soil content is calculated through:

$$SM_v = a \cdot \mathrm{NBMI} + b, \tag{3}$$

where a and b are empirical parameters regressed from in situ soil moisture measurements. This approach estimates soil moisture through change detection rather than a direct relationship between microwave backscattering observations and soil moisture content (Engman, 1990; Kite and Pietroniro, 1996). It is based on an assumption that the change of NBMI is caused solely by the variation of soil moisture, and therefore the effects of other factors including soil texture, surface roughness, and vegetation which are relative temporally consistent are minimized (Engman and Chauhan, 1995).

Although empirical methods can result in an accurate soil moisture retrieval with less complexity and reduced calculation cost than theoretical methods, their applications are restricted in the calibration conditions (Chen et al., 1995; Dubois et al., 1995). To establish a widely applicable empirical

relationship for soil moisture retrieval from radar backscattering observations, a large number of experimental measurements are required (Oh et al., 1992), while current empirical models are generally developed from a limited amount of field measurements and therefore valid only under the specific land surface conditions from which they were derived (Wang and Qu, 2009).

2.3 Semi-empirical approaches

By combining theoretical and empirical approaches, semi-empirical models of backscattering have been developed based on a theoretical foundation with model parameters derived from experimental data.

Oh et al. (1994) developed the first semi-empirical backscattering model, and found that the depolarization ratio (σ_{vh}/σ_{vh}) is very sensitive to soil moisture, and developed a semi-empirical model based on empirical fitting of scatterometer measurements over bare soil surfaces with different roughness conditions. In the Dubois et al. (1995) method, the co-polarized backscattering coefficients σ_{hh} and σ_{vv} are related to the surface dielectric constant, incidence angle, electromagnetic frequency, and root-mean-squared height of soil surface in a nonlinear way.

Compared with empirical models, semi-empirical backscattering models are not expected to have the same site-specific problems (Walker et al., 2004). Generally, these models are more suitable for bare soil surface conditions than vegetated soil conditions.

3 Passive microwave remote sensing

Due to the thermal motion of atoms, any objects at a physical temperature above absolute zero (~−273.15°C or 0 K) radiates electromagnetic energy. A radiometer is used to measure the intensity of this emission, which increases proportionally with the increase in temperature. To explain the relationship between physical temperature and microwave emission, the blackbody concept is used, as introduced by Planck in his quantum theory in 1901. A blackbody is defined as an ideal material that absorbs all incidence radiation and reflects none; it is also a perfect emitter since otherwise its temperature would infinitely increase. Therefore, for a thermodynamic equilibrated blackbody, it emits all absorbed energy outward. In addition, the intensity of electromagnetic emission can be quantified using the term brightness temperature which is defined as the physical temperature of the blackbody emitting the same amount of energy. In contrast to a blackbody, a white body is defined as a perfect reflector that reflects all incidence energy and therefore emits none. Actually, most materials behave between blackbody and white body (refereed as gray body), meaning that a part of incidence energy is reflected with the

remaining absorbed and emitted when at thermodynamic equilibrium. Using the emissivity (*e*) to describe the ability of materials to emit electromagnetic energy, the brightness temperature (*TB*) of the material is expressed as:

$$TB_p = e_p \cdot T, \tag{4}$$

where T is the physical temperature of the material in Kelvin (K), and the subscript p indicates the polarization, either horizontal or vertical. This equation is derived from Plank's blackbody radiation law through the Rayleigh–Jeans approximation for microwave frequencies (Njoku and Entekhabi, 1996; Ulaby et al., 1981b). Therefore, the emissivity of a gray body varies from 0 for a white body to 1 for a blackbody.

For soil material, the emissivity varies from ~0.95 for dry soil (with moisture content of 0.05 m^3/m^3) to ~0.6 for wet soil (with moisture content of 0.4 m^3/m^3), depending on the electromagnetic wavelength, incidence angle, surface roughness, and soil properties (Jackson and Le Vine, 1996; Njoku and Entekhabi, 1996). Assuming soil at a physical temperature of 300 K, this variation in emissivity corresponds to a brightness temperature variation of 90 K (Njoku and Entekhabi, 1996), which is much larger than the typical radiometric sensitivity of microwave radiometers (approximately 1 K).

Following Kirchoff's reciprocity theorem, the microwave emissivity (*e*) of the target can be related to its microwave reflectivity through:

$$\Gamma_p = 1 - e_p. \tag{5}$$

The reflectivity is dependent mainly on the polarization, electromagnetic wavelength, surface roughness, and dielectric constant of materials. For flat specular surfaces, the reflectivity (Γ_p^*) is determined by the Fresnel equation as:

$$\Gamma_H^* = 1 - \left| \frac{\cos\theta - \sqrt{\varepsilon - \sin^2\theta}}{\cos\theta + \sqrt{\varepsilon - \sin^2\theta}} \right|^2 \tag{6}$$

$$\Gamma_V^* = 1 - \left| \frac{\varepsilon \cdot \cos\theta - \sqrt{\varepsilon - \sin^2\theta}}{\varepsilon \cdot \cos\theta + \sqrt{\varepsilon - \sin^2\theta}} \right|^2, \tag{7}$$

where ε is the relative dielectric constant of the material, and θ is the incidence angle of microwave radiation. The subscripts H and V represent horizontal and vertical polarizations, respectively.

The intensity of the emission at microwave frequencies measured by a radiometer, known as brightness temperature, can therefore be related to the dielectric constant through reflectivity. For bare soil with a smooth surface, the emissivity of soil at a given polarization and incidence angle can be determined using Eqns. (5)–(7) from volumetric soil moisture content and soil texture properties. However, for more general land surface conditions, the

effects of temperature profiles in the soil, the roughness of the soil surface, and the vegetation coverage over the soil layer are significant to the relationship between brightness temperature observations and soil moisture (Choudhury et al., 1979; Jackson and Schmugge, 1991; Njoku and Entekhabi, 1996).

3.1 Impact of vertical soil moisture and temperature profiles

In natural land surfaces, soil moisture is not consistent in-depth, and passive microwave observations are only affected by water content in the top soil layer. The effective depth of estimated soil moisture from emitted radiation at microwave frequencies, known as the penetration depth γ_D, is defined as the depth above which soil contributes 63% $(1-1/e)$ of the microwave emission (Ulaby et al., 1981b), and can be expressed as a function of electromagnetic wavelength (λ) and complex dielectric constant of soil $(\varepsilon'_S - j \cdot \varepsilon''_S)$:

$$\gamma_D = \frac{\lambda\sqrt{\varepsilon'_S}}{2\pi\varepsilon''_S}. \tag{8}$$

The penetration depth is very sensitive to the soil moisture conditions, with γ_D varying for L-band from approximately 75 cm for dry soil with a dielectric constant of $5 - j \cdot 0.1$ to approximately 3.7 cm for wet soil with a dielectric constant of $30 - j \cdot 5$. Therefore, the penetration depth is a significant parameter to determine the thickness of the soil surface layer for which the variations in moisture content and temperature make a major contribution to the microwave emission.

The simple relationship of microwave emission in Eqn. (4) is based on an assumption that soil moisture and temperature are constant with depth. At low microwave frequencies, the top several centimeters of soil makes a major impact on the microwave emission (Njoku and Entekhabi, 1996), and in natural soil the vertical distributions of moisture content and temperature can be substantial over this layer, determined by solar radiation, precipitation, evapotranspiration, infiltration rate, and vegetation root distribution. Therefore the uniform soil moisture and temperature profile assumption is not satisfied to estimate soil brightness temperature and emissivity over most natural land surfaces. To account for this variability, an effective soil temperature (T_{eff}), the equivalent temperature in a uniform profile having the same microwave response to the nonuniform temperature profile can be calculated through radiative transfer theory (Choudhury et al., 1982) as:

$$T_{eff} = \int_0^\infty T_S(z) \cdot \alpha(z) \cdot \exp\left[-\int_0^z \alpha(z')\,dz'\right] dz, \tag{9}$$

where $T_S(z)$ is the soil temperature at depth z, and the attenuation coefficient α is dependent on the real and imaginary parts of complex soil dielectric constant as :

$$\alpha(z) = (4\pi/\lambda) \cdot \varepsilon''_S(z)/2 \cdot \left(\varepsilon'_S(z)\right)^{1/2}, \tag{10}$$

where λ is the electromagnetic wavelength. Using this theoretical method, the effective soil temperature can be calculated from the measured soil temperature profile and moisture content, which in turn can be used to estimate the profile of soil dielectric constant. However, the required soil moisture and temperature profile data are only available in limited controlled experiments and so are difficult to obtain over large areas. Therefore, Choudhury et al. (1982) and Wigneron et al. (2001) developed simple linear parameterizations based on Eqn. (9) and experimental data collected at L-band, expressed as:

$$T_{eff} = T_{deep} + C_t \cdot \left(T_{surf} - T_{deep}\right), \tag{11}$$

where T_{deep} and T_{surf} are the deep soil temperature (approximately at 50 cm or 100 cm) and surface temperature (approximately corresponding to a depth interval of 0–5 cm). The parameter C_t is an empirical attenuation coefficient to determine the proportion of the contributions from the deep and surface soil layers to the effective soil temperature. Here the surface temperature can be estimated from thermal infrared observations, or near-surface air temperature derived from meteorological data, while the deep soil temperature can be modeled based on geographic location and season (Choudhury et al., 1982). The constant values of the C_t parameter were calibrated at several frequency bands, and C_t found to be equal to 0.246 at L-band (Choudhury et al., 1982). In reality, the C_t, similar to penetration depth, is also influenced by soil moisture. For very dry conditions, soil layers at depth (deeper than 1 m for dry sand) contribute significantly to the microwave emission from soil, with the C_t being lower than 0.5. In contrast for very wet conditions, the soil emission derives mainly from layers at the soil surface and $C_t \approx 1$. To take the dependence of $C_t$on soil moisture into account, Wigneron et al. (2001) proposed a slightly improved formula based on Eqn. (11) in which C_t is a function of soil moisture:

$$C_t = \left(SM_{surf}/w_0\right)^{b_{w0}}, \tag{12}$$

where SM_{surf} [m^3/m^3] is the volumetric water content in the top 0–3 cm soil. The w_0 [m^3/m^3] and b_{w0} are semi-empirical parameters depending on the soil properties. The long-term suitability of Eqn. (12) was tested over several sites at the seasonal to interannual temporal scales (De Rosnay et al., 2006). The value of w_0 was found to be close to 0.3 m^3/m^3 over two bare soil sites: INRA Avignon (Wigneron et al., 2001) and SMOSREX (De Rosnay et al., 2006). The

value of b_{w0} was close to 0.3 over the INRA Avignon site and close to 0.65 over the SMOSREX site.

3.2 Impact of surface roughness

Generally, natural land surfaces are not flat and smooth like the assumption made in Eqns. (9) and (10). Newton and Rouse Jr (1980) and Wang (1983) found from field measurements that the rougher the soil surface, the higher the soil emissivity and the lower the sensitivity to soil moisture content (see Fig. 3). It was also found that the effects of surface roughness decreased with increased wavelength.

In order to take the effect of surface roughness into account, scattering of the radiation at the soil–air interface was introduced in Eqns. (9) and (10). The reflectivity (Γ_p) of a rough surface generally consists of two components: the noncoherent component (Γ_p^{non}) and the coherent component (Γ_p^{coh}) (Shi et al., 2002). Accordingly, Γ_p^{non} is calculated by integrating over the upper hemisphere bistatic scattering coefficient ($\sigma_{pp}(\vartheta, \vartheta_S, \varphi_S - \varphi)$), which characterizes the scattering of radiation from an incidence direction (ϑ, φ) to the scattered direction (ϑ_S, φ_S):

$$\Gamma_p^{non}(\theta) = 1/(4\pi \cdot \cos\theta) \cdot \int_0^{\pi/2} \int_0^{2\pi} \left(\sigma_{pp}(\theta, \theta_S, \phi_S - \phi)\right) + \sigma_{pq(\theta, \theta_S, \phi_S - \phi)} \sin\theta_S d\phi_S d\theta_S, \quad (13)$$

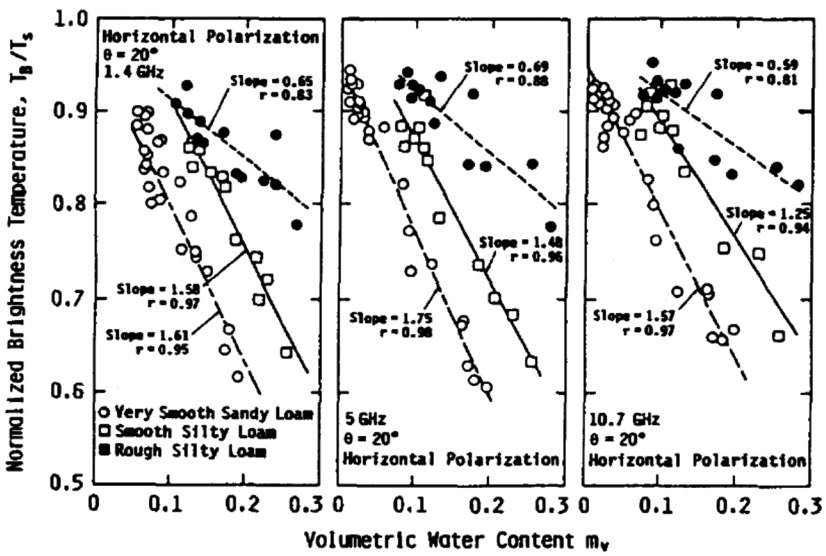

Figure 3 Variations in brightness temperature as a function of moisture content; for soils of different roughness at 1.4 GHz, 5 GHz and 10.7 GHz. Source: Wang et al., (1983).

where the subscripts p and q indicate horizontal and vertical polarizations, or vice versa. The subscript s indicates the direction of the scattered radiation. The bistatic scattering coefficients σ_{pp} and σ_{pq} can be calculated from complex modeling approaches such as the advanced IEM (Chen et al., 2003). The Γ_p^{coh} is expressed as a function of the Fresnel reflectivity (Γ_p^*) such that:

$$\Gamma_p^{coh}(\theta) = \Gamma_p^*(\theta) \cdot \exp\left[-\left(4\pi \cdot SD \cdot \cos\theta/\lambda\right)^2\right] \tag{14}$$

where SD is the standard deviation of the surface height and λ is the electromagnetic wavelength.

This approach is useful to understand the physics of the scattering effect of a rough soil surface. For instance, Shi et al. (2002) demonstrated a large difference in roughness effects at different incidence angles and polarizations. At large incidence angles ($\vartheta \approx 50°$), the soil emission was found to increase as the geometric surface roughness increases at horizontal polarization. This has a good agreement with earlier experimental observations (Choudhury et al., 1979; Wang, 1983; Wang et al., 1983). Conversely, soil emission at vertical polarization decreases as the geometric surface roughness increases. However, this approach does not account for the fine-scale roughness (Schwank and Mätzler, 2006), and only surface scattering effects were considered that ignored volume scattering effects which might substantially affect the soil emissivity. In addition, it is difficult to calculate the emissivity from the scattering coefficients obtained using complex theoretical models and performing a two-dimensional integral on the soil upper hemisphere.

A simple semi-empirical model of soil reflectivity for the rough surface was initially developed by Wang and Choudhury (1981) based on two best-fit parameters Q_R and H_R:

$$\Gamma_P(\theta) = \left[\left(1 - Q_R \cdot \theta_p^*(\theta)\right) + Q_R \cdot \theta_q^*\right] \cdot \exp\left(-H_R \cdot \cos^2(\theta)\right) \tag{15}$$

where the subscripts p and q indicate horizontal and vertical polarizations, or vice versa. The Q_R is a polarization mixing parameter, and the H_R is a surface height parameter that can be related to the SD of surface heights. Wang et al. (1983) considered in a more detailed study that the $\cos\theta$ dependence was much too strong. In addition, H_R in Eqn. (15) increases with surface roughness effects resulting in an increase in soil emissivity at both H and V polarizations, which is in contradiction with theoretical analysis (Mo and Schmugge, 1987; Shi et al., 2002). Consequently, the H_R parameter should be considered as dependent on incidence angle and polarization, and so a generalized semi-empirical equation of roughness effects has been proposed as (Wigneron et al., 2007):

$$\Gamma_P(\theta) = \left[\left(1 - Q_R(\theta)\right)\cdot \Gamma_p^*(\theta) + Q_R(\theta)\cdot \Gamma_q^*\right] \cdot \exp\left(-H_{Rp}(\theta)\cdot \cos^{N_{Rp}}(\theta)\right) \quad (16)$$

In this generalized formulation, the dependence of Q_R and H_R on reflectivity and polarization is accounted for and the N_{Rp} exponent is inserted in the exponential term.

The Q_R was found to be dependent on the electromagnetic frequency and has very small values at L-band (from 0 to 0.12 for three soil types) (Wang et al., 1983). This is in agreement with most of the published studies based on a large experimental data set which considered that $Q_R = 0$ (Mo and Schmugge, 1987; Wegmuller and Mätzler, 1999; Wigneron et al., 2001). The dependence of the model roughness parameter $H_{Rp}(\theta)$ on the surface roughness characteristics, such as SD and autocorrelation length (LC), is not well known. Two studies (Mo and Schmugge, 1987; Wigneron et al., 2001) found that the best geophysical parameters to model H_R were the slope parameter (m = SD/LC) and the surface soil moisture SM. The dependence of H_R on soil moisture content could be explained by a volume scattering effect such that as the soil dries out deeper layers of soil contribute to the emission. Wigneron et al. (2007) suggested that the spatial fluctuations of the dielectric constant within the soil volume may be strong during drying out, having an important 'dielectric' roughness effect, and therefore H_R could be considered as an effective parameter that accounts for (1) 'geometric roughness' effects, corresponding to spatial variations of soil surface height, and (2) 'dielectric roughness' effects, corresponding to the variation of the dielectric constant at the soil surface. The results obtained by Escorihuela et al. (2007) over the SMOSREX (De Rosnay et al., 2006) bare soil confirmed the general soil moisture dependence of H_R and found that a linear dependence was preferable to the exponential one given by (Wigneron et al., 2001).

Wang et al. (1983) found that $N_R = 0$ was consistent with measurements at frequencies of 1.4, 5, and 10.7 GHz. This result was also found in the studies at L-band (Mo and Schmugge, 1987; Wigneron et al., 2001). Based on long-term measurements over a relatively smooth soil during the SMOSREX experiment, Escorihuela et al. (2007) found that $N_R \approx 1$ at horizontal polarization and $N_R \approx -1$ at vertical polarization.

3.3 Impact of vegetation canopy

Over vegetated soil, the microwave emission from the soil layer is affected by the vegetation canopy layer which attenuates (absorbs and scatters) the soil emission and adds its own contribution to the overall microwave emission. As vegetation density increases, the contribution of the vegetation layer increases

and that of the soil layer decreases. When the density of the canopy is adequate, the radiation emitted from the soil layer is masked, and the observed microwave emission relies mainly on the vegetation. The magnitude of the attenuation effect of the canopy depends upon the wavelength and the vegetation water content (VWC).

To date, a number of models have been developed to estimate the microwave emission from the soil-vegetation layer (Jackson et al., 1982; Kirdiashev et al., 1979; Meesters et al., 2005; Mo et al., 1982; Ulaby and Wilson, 1985; Wigneron et al., 1995). In these models, the microwave emission from the vegetated soil surface is usually expressed as a zero-order solution of the radiative transfer equations since it assumes that the scattering phase matrix term can be neglected (Mätzler et al., 2006; Ulaby et al., 1981b, 1982, 1986). The τ - ω model (Mo et al., 1982) is therefore defined as:

$$\begin{aligned} TB_p = &\left(1-\Gamma_p\right)\cdot\gamma_p\cdot T_s + \left(1-\omega_p\right)\cdot\left(1-\gamma_p\right)\cdot T_v \\ &+\left(1-\omega_p\right)\cdot\left(1-\gamma_p\right)\cdot\gamma_p\cdot\Gamma_p\cdot T_v \end{aligned} \tag{17}$$

where T_v and T_s are the effective temperature [K] of the vegetation and soil layers. The ω_p and γ_p parameters are the single scattering albedo and transmissivity of the vegetation layer, respectively, and Γ_p is the reflectivity of a rough soil surface at p polarization (either horizontal or vertical). The microwave emission from a vegetated soil surface is considered as the sum of three parts corresponding to the three terms in Eqn. (17). The first term represents the upward radiation from the soil layer and attenuated by the overlying vegetation. The second term is the upward radiation directly from the vegetation layer. The third term denotes the downward radiation from the vegetation layer, reflected by the soil surface, and attenuated by the vegetation layer again.

The single scattering albedo ω_p indicates the scattering of the soil emissivity, and is a function of vegetation geometry. At microwave frequencies, the value of ω_p is almost zero, varying between 0.05 and 0.10 (Jackson and Schmugge, 1991; Wigneron et al., 2004, 2007). The transmissivity of the vegetation γ_p can be further defined as a function of the vegetation optical depth at nadir (τ_{NAD}) and the incidence angle (θ):

$$\gamma_p = \exp\left[-\tau_{NAD}\cdot\left(tt_p\cdot\sin^2(\theta)+\cos^2(\theta)\right)\cdot\cos^{-1}(\theta)\right] \tag{18}$$

where tt_p is an empirical parameter in relation to vegetation structure and polarization. The optical depth (τ_{NAD}) is dependent on the vegetation density and frequency, and can be linearly related to the VWC (kg/m^2) at L-band using an empirical parameter (b) (Van de Griend and Wigneron, 2004):

$$\tau_{NAD} = b\cdot\mathrm{VWC}. \tag{19}$$

Alternatively, the vegetation optical depth could also be linearly related to the log of the normal difference vegetation index (NDVI) (Burke et al., 2001) using two empirical factors (α and β):

$$\tau_{NAD} = \alpha + \beta \cdot \left(1 - \log\left(\text{NDVI}\right)\right) \tag{20}$$

There is some experimental evidence indicating possible polarization and angle dependence of both τ and ω. However, this dependence was found mainly from experimental data collected over non-isotropic vegetation, such as vertical stalks in tall grasses, grains, and maize (Hornbuckle et al., 2003; Kirdiashev et al., 1979; Wigneron et al., 1995). The canopy and stem structure of most vegetation covers are randomly oriented, and the effects of any systematic orientation of vegetation would be mostly minimized at satellite scales (Martinez-Vazquez et al., 2009; Owe et al., 2001).

For soil moisture retrieval from passive microwave observations of Soil Moisture and Ocean Salinity (SMOS) and SMAP, the vertical temperature gradients within the soil and vegetation layers are assumed uniform, since it reaches equilibrium at around their 6 am/pm overpass times. Therefore, Eqn. (17) can be simplified assuming equaled soil and vegetation temperatures ($T_s = T_v$) (Hornbuckle and England, 2005), expresses as:

$$TB_p = \left[\left(1-\omega_p\right)\cdot\left(1-\gamma_p\right)\cdot\left(1+\gamma_p\Gamma_p\right)+\left(1-\Gamma_p\right)\cdot\gamma_p\right]\cdot T_s \tag{21}$$

The sensitivity of the microwave brightness temperature observation to the water content of the soil layer decreases with the increase of the vegetation opacity depth (Jackson and Schmugge, 1991). The brightness temperature variation reduced by the attenuation effect of the vegetation canopy is much larger than the noise sensitivity threshold of a microwave radiometer (typically <1 K). Therefore, the passive microwave technique can obtain a large signal-to-noise ratio (SNR) for accurate soil moisture remote sensing.

4 Remote sensing of soil properties

Remote sensing is a means to acquire information about an object by measuring its emitted, reflected, and/or scattered radiation from a distance without physical contact. Based on the provision of radiation sources, remote sensing techniques can be divided into active and passive categories. Active remote sensing measures the radiation emitted primarily from an illumination source, but also secondary reflection/scattering from surface of the sensed object. In contrast, passive remote sensing only measures the self-emitted radiation from the sensed object due to its inherent physical temperature, which normally has a lower SNR than active remote sensing. In most cases, the remotely sensed radiation is in the form of electromagnetic waves, but other forms (e.g. acoustic

wave, neutron scattering, gamma attenuation, and gravity change) can also be used for ground, airborne, and satellite remote sensing. According to the electromagnetic frequency spectrum, remote sensing can be categorized into optical and microwave remote sensing. Optical remote sensing has a high spatial resolution and a high spectral resolution, with current optical remote sensing satellites reaching submeter (<1 m) spatial resolutions (e.g. WorldView, GeoEye, QuickBird, Ikonos, Pleiades,GF-2, and KF01) and ~10 nm spectral resolutions (e.g. MightSat-II, EO-1, PROBA, ENVISAT-1, MRO, HySI, TacSat-3, HICO, GOSAT, OCO-2, and EnMAP). However, optical imagery is adversely affected by the atmosphere and clouds, temporal repeat, and its inability to penetrate the land surface cover. With longer wavelength, microwave remote sensing has a high penetration capability and a sensitivity to target dielectric constant. But microwave sensors require a larger antenna and achieve a lower spatial resolution. Being limited by current antenna technology, the best spatial resolution that can be achieved by L-band (1–2 GHz) radiometers from the space is only ~40 km (e.g. SMOS and SMAP).

4.1 Soil moisture

Extensive research has been conducted on soil moisture retrieval from remote sensing techniques over the past four decades, with the main difference in techniques being the measured frequency within the electromagnetic spectrum and the source of the radiation. Optical methods exploit the relationship between soil moisture and spectral reflectance in the visible/near-infrared bands to empirically determine the soil moisture in the top millimeters or so of the soil surface, while thermal infrared-based methods start from capturing the thermal inertia of soil which is then related to the soil moisture through the thermal conductivity and/or the heat capacity (Petropoulos et al., 2015). In general, the absorption of visible bands increases as soil moisture is increased, resulting in a decrease of reflectance at visible bands (Gao et al., 2013; Liu et al., 2002). However, this tenuous relationship and the optimal spectrum bands vary significantly from site to site (Liu et al., 2009), because of the additional dependence of reflectance on organic matter content, roughness, texture, and observation geometry (Petropoulos et al., 2015). Moreover, the optical and thermal signal has limited capability to penetrate cloud and vegetation, requiring careful correction to eliminate atmospheric effects (Zhao and Li, 2013). These are the main reasons for limited use of visible/thermal bands in soil moisture retrieval, despite the multitude of optical sensors currently available.

The microwave technique has been widely acknowledged as the most promising for near-surface soil moisture mapping at regional to global scales, due to its penetration capability of the vegetation layer, independence of

solar illumination, and direct relationship to soil moisture via the dielectric constant (Ulaby et al., 1981a). The microwave radiometers operating at higher frequency such as C-band (i.e. AMSR-E, Wind-Sat), or X-band (i.e. TMI) are also sensitive to soil moisture, however, microwave emission from the soil layer at these wavelengths is significantly affected by attenuation from the vegetation canopy and scattering by the atmosphere. Since the penetrability of microwave radiation is dependent mainly on the wavelength of the signal, microwave radiometers at these higher frequencies need to account for the atmospheric contribution, are only sensitive to water content in the top less than 1 cm layer of soil, and are limited to areas with low vegetation cover (VWC < 3 kg/m^2). In contrast, L-band radiometer observations are unaffected by the atmosphere, able to penetrate the top ~5 cm layer of soil, and sensitive to soil moisture with vegetation coverage of up to ~5 kg/m^2, corresponding to about 70% of the nonfrozen land regions on Earth, excluding dense forests. Consequently, passive microwave at L-band (~1.4 GHz) is considered the most promising remote sensing technique for near-surface soil moisture mapping at regional to global scales. Not only due to its penetration capability of cloud and vegetation, but also its independence of solar illumination, direct relationship with volumetric soil moisture through the soil dielectric constant, and reduced sensitivity to land surface roughness and vegetation cover (Jackson and Schmugge, 1989; Njoku et al., 2002; Schmugge et al., 1986; Shutko and Reutov, 1982; Ulaby et al., 1981b).

The first space-borne passive microwave observations at L-band were collected by the SkyLab mission within a limited duration in the 1970s, being the earliest demonstration of soil moisture retrieval from passive L-band observations from space (Jackson et al., 2004). However, the first satellite dedicated to soil moisture was not launched until November 2009, carrying a 2D interferometric radiometer to measure microwave emission from the Earth surface at L-band (1.413 GHz). Development of the SMOS mission was led by the ESA, aiming to map global soil moisture every 2–3 days with a target accuracy of 0.04 m^3/m^3 (Kerr et al., 2010). Additionally, the Soil Moisture Active and Passive (SMAP) mission developed the National Aeronautic and Space Administration was launched in January 2015, designed to combine L-band radiometer (1.41 GHz) and radar (1.26 GHz) instruments in order to achieve soil moisture retrieval with the same target accuracy as SMOS but at an enhanced special resolution (Entekhabi et al., 2010).

Based on the current level of antenna technology, the spatial resolution of space-borne radiometers is limited to around 40 km. For a higher spatial resolution, extensive research has been conducted using active microwave data, especially the data collected by SAR. A SAR is a coherent mostly side-looking radar system that utilizes signal processing and the movement of the

platform to simulate an extremely large antenna or aperture, resulting in a high resolution in azimuth (up to half of the real aperture length) (Ulaby et al., 2014). Over land surfaces, a part of the transmitted electromagnetic wave is scattered by the vegetation canopy and/or soil surface, and returned back to the SAR system (known as backscatter). In general, backscatter increases as soil moisture (relative permittivity) is increased, and thus soil moisture can be inverted from scattering models describing this relationship. The commonly used scattering models include the IEM (Fung, 1994a) for bare soil and the water cloud model (Attema and Ulaby, 1978) for vegetated areas.

Apart from soil moisture, radar measurements are also sensitive to soil surface roughness and vegetation parameters, which results in high uncertainty in the soil moisture retrieval algorithms for SAR observations (Ulaby et al., 2014). To decouple the effect of soil roughness and vegetation, some studies decomposed the received signal into individual contributions of the soil surface, vegetation and multiple scattering between soil surface and vegetation, with soil moisture then being retrieved from the soil surface contribution (Hajnsek et al., 2009; Jagdhuber et al., 2013). Some other studies assume that roughness and vegetation do not change between repeat passes of radar observations, and thus the difference of backscatter can be empirically related to the variation of soil moisture (Wagner et al., 1999a,b). This assumption was also used to remove the unknowns representing the temporal variation of roughness and vegetation, resulting in a well-constrained inversion process (Kim et al., 2012; Zhu et al., 2019b). While space-borne SAR has shown promising results for soil moisture retrieval at high spatial resolution (0.1–1 km), it suffers from a narrow beamwidth that cannot satisfy the temporal and global coverage requirements of hydrology applications (~3 days). Currently, only the Sentinel-1 (Torres et al., 2012), SAOCOM, PALSAR-2 (Kankaku et al., 2014), Biomass mission (Le Toan et al., 2011), and NIRSAR (Rosen et al., 2017) can plan to provide regular global observations, however, their repeat coverages range from 6 days to 60 days. Algorithms that can merge data from multiple SAR missions was thus proposed recently to enhance the revisit (Zhu et al., 2019a).

4.2 Soil roughness

The collected radar signal is heavily dependent on surface roughness. When a wave impinges on a smooth soil surface, some of the energy is scattered in non-specular directions, with a small amount returning to the radar as backscatter. As surface roughness increases, the amount of reflection in the specular direction decreases, and consequently the surface scattering increases (Ulaby et al., 2014). Radar measurements are thus an effective venue to characterize surface roughness. In general, the soil surface is described either as a one-scale

stationary random process or a random process superimposed on a periodic surface for periodic plowed surfaces (Ulaby et al., 2014). For random surfaces, two parameters describing the vertical (RMS height) and horizontal (correlation length) variation are commonly used, while a few extra parameters (e.g. the period, orientation, and the maximum height of the periodic surface) are required for periodic plowed surfaces. These parameters are well considered in various surface scattering models, e.g. the IEM (Fung, 1994a) and the multi-scale IEM (Monsivais-Huertero et al., 2018). Roughness can thus be estimated by inverting these scattering models with or without ground soil moisture measurements (Zhu et al., 2019a). However, the use of ground-measured roughness parameters commonly result in substantial inconsistency between the modeled and observed radar observation (Baghdadi et al., 2002; Lievens et al., 2011; Zhu et al., 2016), suggesting that the RMS height and correlation length cannot represent the roughness perceived by radar systems. Accordingly, the roughness values estimated from radar data are effective without a determined physical definition. Moreover, many studies have confirmed that the effective roughness varies at different radar frequency bands and incidence angles. For example, larger effective roughness values were observed at lower incidence angles over the same location (Baghdadi et al., 2006; Lievens et al., 2011; Martinez-Agirre et al., 2017). The use of radar-based roughness in other applications is still questionable.

4.3 Soil salinity

The presence of salt in the shallow Earth surface can be detected by remote sensing either directly on bare soil, or indirectly through the vegetation type and growth that is controlled or affected by the salinity. Salt mineralogy determines the presence or absence of absorption in optical bands (Metternicht and Zinck, 2008), while the microwave spectrum is mainly affected by the quantity of salt in the soil water (Lasne et al., 2008). Salts also cause variations of surface roughness. For example, the concentration of salt at the soil surface can result in smooth surfaces (e.g. puffy crusts), leading to higher reflectance in the optical bands but lower emissivity and backscatter in the microwave spectrum than nonsaline and cultivated surfaces (Metternicht and Zinck, 2008).

Optical remote sensing is mainly used to capture the spatial pattern of salt-affected surface features and their temporal evolutions, with some sophisticated remote sensing indexes (Khan et al., 2005; Sidike et al., 2014; Wang et al., 2019) proposed for aerial photos, high spatial resolution satellite imagery (e.g. WorldView series), and sensors with a wider spectrum up to 2500 nm (e.g. Landsat series and Sentinel-2). The end of dry season is widely recognized as the optimal time slot for salinity mapping as salts dissolve during the rainy season

(Metternicht and Zinck, 2003; Wang et al., 2019). In contrast, some soil moisture is required for microwave-based remote sensing, as the measurements are mainly dependent on dielectric constant determined by moisture and salt that dissolved in moisture (Ulaby et al., 2014). Previous studies using microwave data have mainly focused on (1) saline water detection in water logging areas by analyzing the dependence of brightness temperature on temperature and salinity (Singh and Srivastav, 1990); and (2) soil salinity mapping by relating the imaginary part of the dielectric constant with measured backscatter (Bell et al., 2001; Periasamy and Ravi, 2020; Taghadosi et al., 2019). The presence of halophytic salt-tolerant vegetation interferes with the reflectance, emissivity, or backscatter of salinity features, being more challenging for direct salinity mapping. The type of vegetation and its growth however provide alternative indicators of soil salinity. For example, the health status of cotton plants and cotton yield have strong correlation with electrical conductivity (Metternicht and Zinck, 2003).

Despite the great advance, precise estimation of salt quantities from remote sensing is rather challenging due to the multiple dependence of remote sensing data on surface parameters, e.g. soil moisture, soil texture, roughness, organic matter (Jackson and O'Neill, 1987; Petropoulos et al., 2015). Ground samples remain necessary to provide required field data (e.g. water table depth and salinity data) and is still the basis of empirical relationships between remote sensing data and salinity features.

5 Case study

5.1 Murrumbidgee River Catchment

The Murrumbidgee River Catchment is located in southeast of Australia, with an area of ~82 000 km^2, and an elevation ranging from ~40 m in the western plains to ~2000 m in the eastern mountainous areas as shown in Fig. 4. The annual rainfall varies from 300 mm in the west to 1900 mm in the high elevated ranges in the east (Australian Bureau of Rural Science, 2001). Accordingly, the land surface of the Murrumbidgee River Catchment varies from bare soil with sparse vegetation in the west, to irrigated fields mixed with grasslands in the middle, and to forest in the east. Due to the variability in topography, climate, land cover, and soil textures of the Murrumbidgee catchment, the long-term hydrological monitoring network: OzNet (Smith et al., 2012) has been operating for 15 years. At the same time, a series of airborne field experiments have been conducted for the development of soil moisture remote sensing techniques, such as NAFE'05 (Panciera et al., 2008), NAFE'06 (Merlin et al., 2008), AACES-1/-2 (Peischl et al., 2012), SMAPEx-1 to -3 (Panciera et al., 2014), and SMAPEx-4/-5 (Ye et al., 2021).

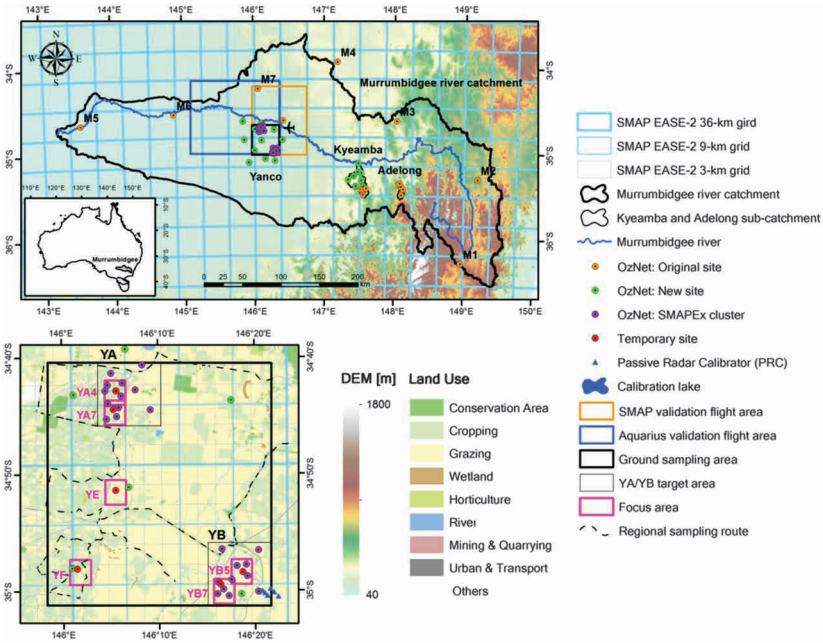

Figure 4 Location of the OzNet monitoring stations and the SMAPEx-4/5 study area in the Murrumbidgee River Catchment with the digital elevation model (DEM) and the SMAP EASE-2 grid at 36 km scale as backdrop (top). Layout of the ground sampling focus areas and monitoring stations with land use map and the SMAP EASE-2 grids at 9 km and 3 km scales as backdrop (bottom). Source: Adapted from Ye et al. (2021).

5.2 Soil moisture active passive experiments

The soil moisture active passive experiments (SMAPEx) comprised a series of five airborne field campaigns for calibration and validation of SMAP under Australian land surface conditions. The first three experiments (SMAPEx-1 to -3; Panciera et al., 2014) were conducted between July 2010 and September 2011, for the development of SMAP prelaunch soil moisture retrieval and downscaling algorithms. The SMAPEx-4 and -5 (Ye et al., 2021) were conducted at the beginning of the SMAP operational phase in May and September 2015 respectively, for in-orbit validation of the SMAP observations and soil moisture products in different seasons. The specific objectives were to: (1) evaluate SMAP active-passive downscaled 9 km radiometer observations; (2) inter-compare SMAP, SMOS, and Aquarius with airborne radiometer/radar observations; (3) validate SMAP radar-only, radiometer-only, and radar-radiometer soil moisture retrieval algorithms using airborne soil moisture retrieval results from field experiments and long-term soil moisture monitoring network measurements; and (4) further develop radar-only soil moisture retrieval algorithms.

A flight area of 71 km × 89 km was identified over the Yanco area (Fig. 4), and airborne active and passive microwave observations were collected coincident with SMAP coverage during 3 weeks in each experiment. The main airborne instruments used in the SMAPEx-4 and -5 were the Polarimetric L-Band Multi-beam Radiometer (PLMR) and the Polarimetric L-band Imaging Synthetic (PLIS) aperture radar, which operate at the same frequencies of the SMAP radiometer and radar, respectively. During the 3 weeks period of SMAPEx-4, eight flights were taken over two study areas according to the 3 dB footprints of the SMAP and Aquarius radiometers, respectively (Fig. 4). Airborne PLMR brightness temperature observations at 1 km resolution and airborne PLIS backscatter observations at ~30 m resolution were collected in each flight between 3 am and 9 am (local time), in alignment with the SMAP nominal local overpass time of 6 am. Figure 5 shows an example of PLMR brightness temperature normalized to 38.5°and PLIS backscatter normalized to the reference incidence angle of SMAP (40°), using the Ye et al. (2015) approach. Ground sampling of the top 5 cm soil moisture, VWC, and surface roughness were collected concurrently with airborne sampling over the six 3 km focus areas (Fig. 4), in order to provide spatial soil moisture data for validation and the ancillary data used in soil moisture retrieval. Prior to SMAPEx-4 and -5, heavy rainfall events occurred and were followed by a drying out period, providing ideal opportunities to validate SMAP products under a variety of soil moisture, land surface types, and topography conditions. A total of 16 flights were conducted during the SMAPEx-4 and -5.

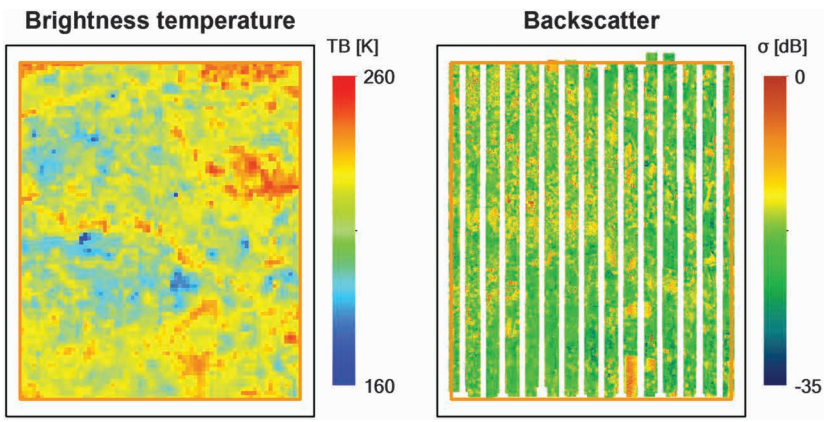

Figure 5 Maps of airborne brightness temperature normalized to 38.5° (left) and backscatter observations normalized to 40° (right) over the SMAP validation flight area on 11 May 2015. Source: Adapted from Ye et al. (2021).

5.3 Passive microwave remote sensing of soil moisture

Airborne soil moisture was retrieved from the dual-polarized PLMR brightness temperature observations using the L-MEB model (Wigneron et al., 2007). The VWC was estimated from the MODIS 250 m daily reflectance products (MOD09GQ) using the Gao et al. (2015) method. The required roughness and vegetation parameters in the L-MEB were adapted from previous studies in the Yanco area (Panciera et al., 2008, 2009) and literature (Grant et al., 2008; Wigneron et al., 2007). The surface and deep soil temperatures were obtained from monitoring stations and used to estimate effective temperature in Eqn. (14). The retrieved soil moisture data were validated using the ground 250 m spacing soil moisture measurements over all six focus areas. According to the comparison results shown in Fig. 6, an overall RMSE of 0.08 m^3/m^3 was achieved for SMAPEx-4/-5 soil moisture data at 1 km scale, while soil moisture was overestimated in SMAPEx-5 in some instances due to the presence of standing water.

Figure 7 shows the temporal variation of top 5 cm soil moisture retrieved from the 1 km PLMR brightness temperature observations across the SMAPEx-4 and -5, respectively. As the result of two rainfall events, 9 May and 18 May 2015, soil moisture over the flight area varied from a dry homogeneous condition to a heterogeneous spatially distributed pattern during the SMAPEx-4. The SMAPEx-5 started from a very wet and partly flooded condition on 8 September 2015, and experienced a drying out period to the end of the experiment on 26 September 2015. The 1 km PLMR-derived soil moisture data were averaged

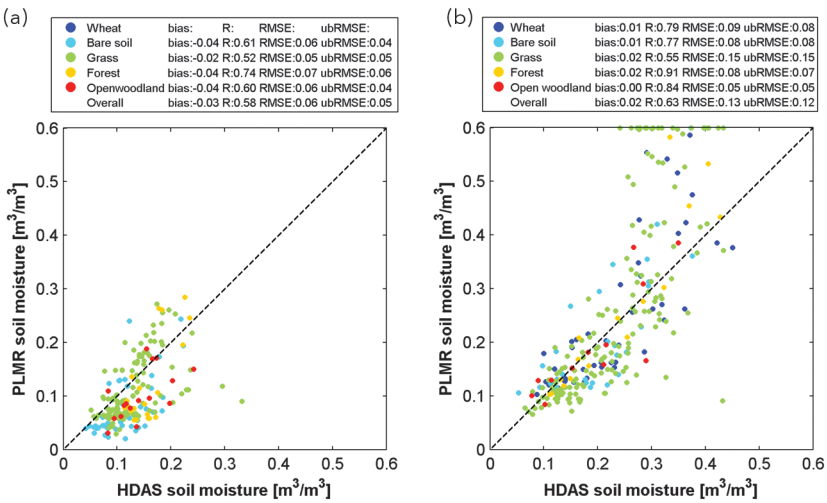

Figure 6 Comparison between top 5 cm soil moisture measurements and soil moisture retrieved from the 1 km PLMR brightness temperature observations during SMAPEx-4 (a) and -5 (b) using published parameters. Source: Adapted from Ye et al. (2021).

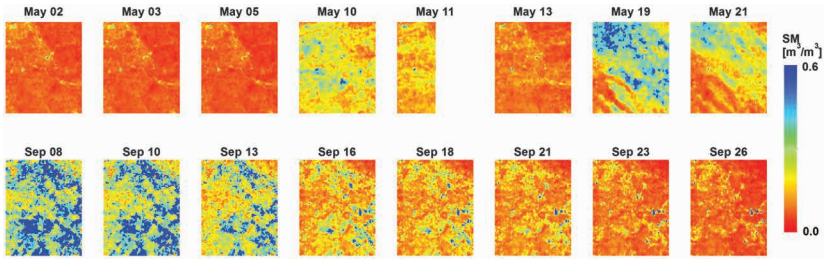

Figure 7 Maps of 1-kmPLMR-derived soil moisture over the SMAP validation flight area during the SMAPEx-4 (top) and -5 (bottom).

to the SMAP EASE grids at 3 km, 9 km, and 36 km, and then compared with SMAP soil moisture products at pixel levels as shown in Fig. 8. Taking the PLMR soil moisture as the reference, the SMAPL2 Passive, Active-Passive downscaled, and Active soil moisture products had high correlations with RMSEs of ≤0.04 m^3/m^3, 0.07 m^3/m^3, and 0.11 m^3/m^3 in both SMAPEx-4 and -5. Consequently, the SMAPEx-4 and -5 data sets demonstrate the capability of monitoring temporal and spatial variation of near-surface soil moisture using microwave remote sensing technique, and provided airborne brightness temperature and backscatter observations for the validation of SMAP.

5.4 Radar remote sensing of soil moisture

Radar data collected across the SMAPEx-5 campaign, covering three frequency bands (aircraft and satellite), L-, C-, and X-band with varying incidence angle and polarizations over time, were used for soil moisture retrieval here. Radar data were available for 15 days of the 3-week campaign, being a simulation of the dense data expected from combining recent and projected radar satellite missions. The available observations varied from day to day, with 5 and 10 days

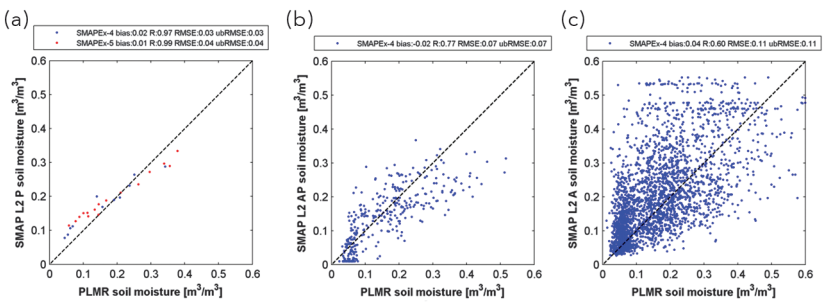

Figure 8 Comparison of SMAPEx-4 and -5 airborne PLMR soil moisture versus SMAPL2 Passive/radiometer (a), Active-Passive downscaled (b), and Active/radar (c) products. Source: Referred from Ye et al. (2021).

Table 2 The main components of the stochastic ensemble framework

Component	Description	Reference
Scattering models	Three frequency-specific look up tables (LUTs) built by NMM3D and distort Born approximation, representing the relationships between soil moisture, roughness, and radar observations.	Zhu et al. (2019b)
Change detection component	It implements an unsupervised change detection of the areas with roughness and/or vegetation changes, being a preprocessing procedure.	Zhu et al. (2019c)
Channel selection	It estimates the contribution of vegetation volume scattering and removes the channels dominated by volume scattering.	Zhu et al. (2019a)
Ensemble retrieval	It implements multiple soil moisture retrievals using random subsets of input radar data and get their ensemble average as the output.	Zhu et al. (2020)

having dual-frequency (L + C or C + X) and single-frequency data, respectively. A stochastic ensemble framework was proposed for soil moisture retrieval, with the main components summarized in Table 2.

Soil moisture retrieval was made at the 25 m pixel and paddock scales, respectively, using all available radar data. The 25-m pixel soil moisture maps for the YA4 area are depicted in Fig. 9 as an example, while the paddock scale

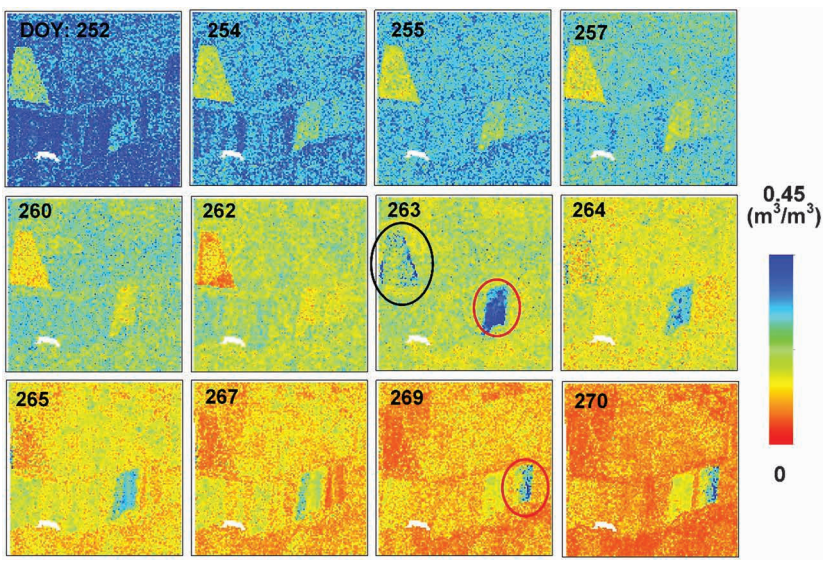

Figure 9 Retrieved soil moisture maps in YA4 with the day of year listed in top left. The paddocks in black circles are these with soil plowing, while the red circles are those with irrigation.

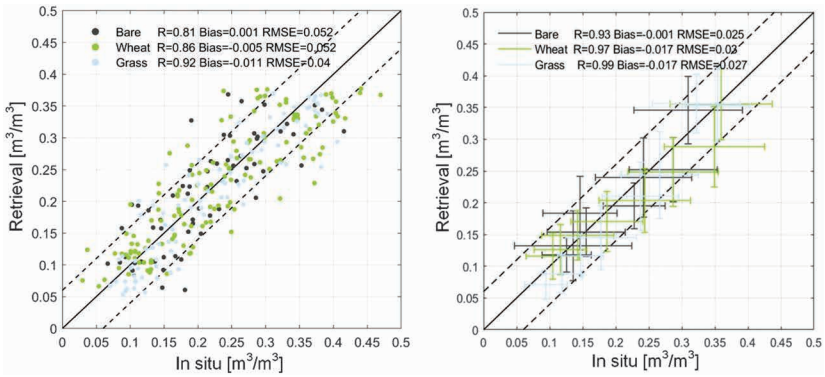

Figure 10 *In situ* versus retrieved soil moisture at the paddock scale (left panel) and daily average (right panel) using time series L-, C-, and X-band data. The dashed lines denote the ± 0.06 cm^3/cm^3.

and daily average comparison against corresponding ground measurements are shown in Fig. 10. The retrieved time series soil moisture maps agreed well with the dry down process observed during SMAPEx-5, with a faster dry down observed over bare soil paddocks. The observed cultivation activities in the circled paddocks were detected, with the sudden soil moisture increases being successfully recorded.

Moderate accuracy was achieved at the paddock scale, showing an RMSE of 0.04–0.06 m^3/m^3 and a correlation coefficient (R) of 0.8–0.9, reaching the 0.06 m^3/m^3 accuracy target of SMAP radar products. The retrieved soil moisture for wet conditions (larger than 0.4 m^3/m^3) was slightly underestimated. Such underestimations were also observed and ascribed to the decreased sensitivity of σ^0 in moist areas in other studies (Bai et al., 2016; Wang et al., 2011). Another interpretation could be the relatively low upper bound of soil moisture in the LUTs (~0.43 m^3/m^3) compared to the ground measurements during the first days of SMAPEx-5. As expected, the results were greatly improved for daily average values. The RMSE decreased to 0.025 m^3/m^3, 0.03 m^3/m^3, and 0.027 m^3/m^3 in bare, wheat, and grass, respectively. A good correlation (R: 0.93–0.99) was observed with negligible bias (<0.02 m^3/m^3). The retrieved accuracy was much better than the requirement of 0.05 m^3/m^3 suggested by Walker and Houser (2004) and World Meteorological Organization (available at http://www.wmosat.info/oscar/requirements).

5.5 Irrigator/tower/unmanned aerial vehicle-based remote sensing of soil moisture

Soil moisture is a temporal and spatially varying variable that plays an important role in the agriculture industry. Although the current level of irrigator technology

supports the precise control of the volume of irrigation water, it is difficult to accurately estimate spatial irrigation water demand, due to the high spatial variability of soil moisture. Therefore, the efficiency of irrigation water use can be improved by introducing real-time soil moisture mapping to determine the spatial distribution of required irrigation water volume, and an irrigation-based soil moisture remote sensing experiment has been conducted to demonstrate this potential. The irrigator-based passive microwave soil moisture experiment was conducted over a 200 m by 600 m farm near Cora Lynn, in southeast of Australia (Fig. 11). The ELBARA III (the Eidgenössische Technische Hochschule [ETH] L-band radiometer for soil moisture research; Jonard et al., 2011; Schwank et al., 2010) was mounted on an irrigation boom with a 40° incidence angle and a 5 m footprint. Dual-polarized brightness temperature observations were collected over a 5 m by 600 m transect when the irrigator moved across the farm.

To validate soil moisture retrieval accuracy, point-based soil moisture measurements were collected at the same time using the Hydraprobe Data Acquisition System (HDAS) (Merlin et al., 2007; Panciera et al., 2006). Figure 12 shows the spatial distribution of soil moisture data measured using the HDAS and retrieved from the ELBARA III brightness temperature observations, respectively. Soil moisture was found to have a considerable variation of

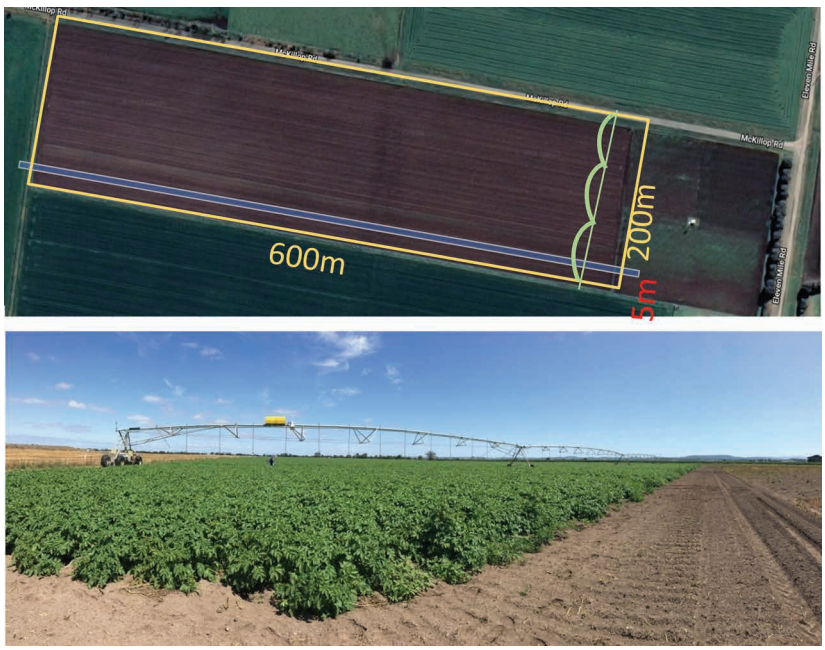

Figure 11 Overview of the irrigator-based soil moisture remote sensing experiment (top) and picture of the irrigator with the ELBARA III mounted on the boom.

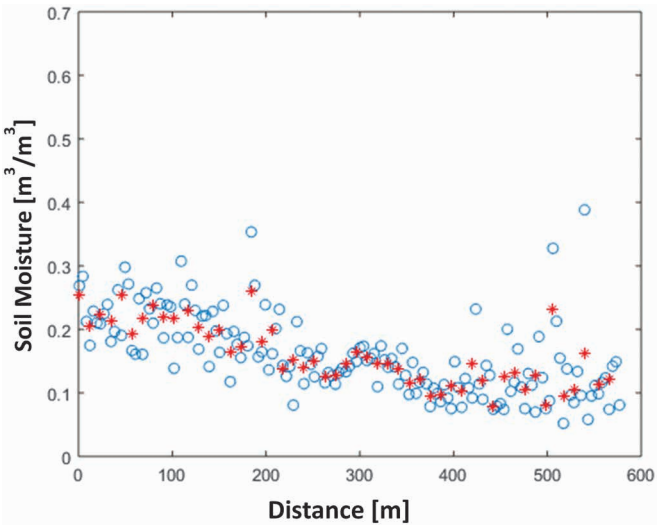

Figure 12 Soil moisture measurements along the ELBARA III transect. The red dots and blue circles indicate soil moisture data measured using the HDAS and retrieved from the ELBARA III brightness temperature observations respectively.

more than 0.2 m^2/m^2 within the same farm, although normally assumed as a homogeneous condition. This confirms the difficulty to accurately measure soil moisture at farm scales using conventional methods, and thus the potential of saving irrigation water by accounting for initial soil moisture using remote sensing techniques. The ELBARA III-derived soil moisture had a similar spatial pattern and a high correlation to the HDAS soil moisture measurements, demonstrating the applicability of boom-based passive microwave soil moisture remote sensing application in the agriculture industry.

6 Future trends in research

With the recent development of sensor technology, the sizes and costs of sensors have been reduced significantly, such that a series of portable sensors have been employed on different platforms including unmanned aerial vehicle (UAV). Compared with traditional aircraft (Bai and Purcell, 2018; Bellvert et al., 2015; Gerhards et al., 2018; Walker et al., , 2012; Zhang et al., 2017) and satellite (Calera et al., 2017; Du et al., 2013; Helman et al., 2018) platforms, UAVs are small, inexpensive, easy, and autonomous, providing a new remote sensing platform with an improved spatial resolution and sampling flexibility in precision agriculture application (Vergara-Díaz et al., 2016; Zarco-Tejada et al., 2009, 2013). The optical remote sensing techniques has been tested for UAV-based surface soil moisture mapping (e.g. Hassan-Esfahani et al., 2014; Hoffmann et al., 2016; Lu et al., 2020; Turner et al., 2011). To overcome the

limitation of optical techniques on soil moisture remote sensing, only a few passive microwave sensors have been developed for UAV-based soil moisture mapping (Acevo-Herrera et al., 2010; Houtz et al., 2020). However, it can be expected in the future that L-band passive microwave remote sensing with a high sensitivity to soil moisture will be used together with the optical technique on UAVs to map high-resolution soil moisture at farm scale.

The state-of-art L-band passive microwave soil moisture remote sensing technique is limited to measure water content in the top ~5 cm of the soil. According to theoretical and experimental studies (Laymon et al., 2001; Njoku and Entekhabi, 1996; Shi et al., 2005), the sensing depth of passive microwave sensors is a function of the wavelength. Thus a deeper layer of soil can be achieved by using radiometers at lower frequencies (Njoku et al., 2003; Njoku and Kong, 1977; Paloscia et al., 1993). In addition, the impacts of surface roughness and overlaying vegetation on soil moisture retrieval accuracy are expected to be reduced. Consequently, a radiometer with a doubled wavelength (40 cm) operating at P-band (750 MHz) has been developed to demonstrate the capability of measuring a deeper layer (~10 cm) soil moisture over more densely vegetated surfaces, and with overall improved accuracy. Currently, a series of tower-based and airborne field experiments are being conducted to explore the potential of P-band passive microwave soil moisture remote sensing. The initial results show a higher sensing depth, less sensitivity on vegetation and roughness, and higher accuracy for P-band than L-band soil moisture remote sensing (Shen et al., 2020; Ye et al., 2020).

With the increasing availability of 'Earth big data', the use of deep learning in soil characteristics mapping has attracted broad attention in recent years (Yuan et al., 2020). Deep learning models can accurately approximate the complicated nonlinear relationship between soil characteristics and various remote sensing observations, without requiring cumbersome physical modeling and the ill-posed inversion process (Ali et al., 2015; Notarnicola et al., 2008). A neural network has been successfully applied to global soil moisture mapping from passive microwave data (Rodriguez-Fernandez et al., 2015) and some regional-scale applications (Rodríguez-Fernández et al., 2017; Santi et al., 2016). However, the ground truth for training is either from climate models (e.g. the European Centre for Medium-Range Weather Forecasts model) or in situ measurements. Currently, the main limitation of deep learning is that the limited in situ measurements (Dorigo et al., 2021) cannot reach the requirement of training a deep and wide neural network, with the trained neural network being too simple to have satisfactory accuracy and generalization capability. Theories and/or techniques (e.g. transfer learning) that can be used to provide more samples and/or reduce the number of required ground samples are thus expected to be the key to further use of deep learning in soil mapping.

7 Where to look for further information

The following articles provide a good overview of the subject:

- Ulaby, F. T., Long, D. G., Blackwell, W. J., Elachi, C., Fung, A. K., Ruf, C., Sarabandi, K., Zebker, H. A. and Van Zyl, J. (2014). *Microwave Radar and Radiometric Remote Sensing*. Ann Arbor: The University of Michigan Press.

Key research in this area can be found at the following organizations:

- Department of Civil Engineering, Monash University.
- https://www.monash.edu/engineering/jeffwalker.
- https://www.researchgate.net/profile/Jeffrey-Walker-9.

8 References

Acevo-Herrera, R., Aguasca, A., Bosch-Lluis, X., Camps, A., Martínez-Fernández, J., Sánchez-Martín, N. and Pérez-Gutiérrez, C. (2010). Design and first results of an UAV-borne L-band radiometer for multiple monitoring purposes. *Remote Sensing* 2(7), 1662–1679.

Ali, I., Greifeneder, F., Stamenkovic, J., Neumann, M. and Notarnicola, C. (2015). Review of machine learning approaches for biomass and soil moisture retrievals from remote sensing data. *Remote Sensing* 7(12), 16398–16421.

Attema, E. P. W. and Ulaby, F. T. (1978). Vegetation modeled as a water cloud. *Radio Science* 13(2), 357–364.

Australian Bureau of Rural Science. (2001). *Mean Monthly and Mean Annual Rainfall and Temperature Data*. Melbourne, Australia: Bureau of Meteorology.

Baghdadi, N., Holah, N. and Zribi, M. (2006). Calibration of the integral equation model for SAR data in C-band and HH and VV polarizations. *International Journal of Remote Sensing* 27(4), 805–816.

Baghdadi, N., King, C., Chanzy, A. and Wigneron, J. P. (2002). An empirical calibration of the integral equation model based on SAR data, soil moisture and surface roughness measurement over bare soils. *International Journal of Remote Sensing* 23(20), 4325–4340.

Bai, X., He, B. and Li, X. (2016). Optimum surface roughness to parameterize advanced integral equation model for soil moisture retrieval in prairie area using Radarsat-2 data. IEEE Transactions on Geoscience and Remote Sensing 54, 2437–2449.

Bai, H. and Purcell, L. C. (2018). Aerial canopy temperature differences between fast-and slow-wilting soya bean genotypes. *Journal of Agronomy and Crop Science* 204(3), 243–251.

Beckmann, P. and Spizzichino, A. (1963). *The Scattering of Electromagnetic Waves From Rough Surfaces*. Norwood, MA: Artech House, Inc.

Bell, D., Menges, C., Ahmad, W. and Van Zyl, J. J. (2001). The application of dielectric retrieval algorithms for mapping soil salinity in a tropical coastal environment using airborne polarimetric SAR. *Remote Sensing of Environment* 75(3), 375–384.

Bellvert, J., Marsal, J., Girona, J. and Zarco-Tejada, P. J. (2015). Seasonal evolution of crop water stress index in grapevine varieties determined with high-resolution remote sensing thermal imagery. *Irrigation Science* 33(2), 81–93.

Burke, E. J., Shuttleworth, W. J. and French, A. N. (2001). Using vegetation indices for soil-moisture retrievals from passive microwave radiometry. *Hydrology and Earth System Sciences* 5(4), 671–678.

Calera, A., Campos, I., Osann, A., D'Urso, G. and Menenti, M. (2017). Remote sensing for crop water management: From ET modelling to services for the end users. *Sensors* 17(5), 1104.

Chen, K. S., Wu, Tzong-Dar, Tsang, Leung, Li, Qin, Shi, Jiancheng and Fung, A. K. (2003). Emission of rough surfaces calculated by the integral equation method with comparison to three-dimensional moment method simulations. *IEEE Transactions on Geoscience and Remote Sensing* 41(1), 90–101.

Chen, K. S., Yen, S. K. and Huang, W. P. (1995). A simple model for retrieving bare soil moisture from radar-scattering coefficients. *Remote Sensing of Environment* 54(2), 121–126.

Choudhury, B. J., Schmugge, T. J., Chang, A. and Newton, R. W. (1979). Effect of surface roughness on the microwave emission from soils. *Journal of Geophysical Research* 84(C9), 5699–5706.

Choudhury, B. J., Schmugge, T. J. and Mo, T. (1982). A parameterization of effective soil temperature for microwave emission. *Journal of Geophysical Research* 87(C2), 1301–1304.

D'urso, G. and Minacapilli, M. (2006). A semi-empirical approach for surface soil water content estimation from radar data without a-priori information on surface roughness. *Journal of Hydrology* 321(1–4), 297–310.

De Rosnay, P., Wigneron, J.-P., Holmes, T. and Calvet, J.-C. (2006). Parameterizations of the effective temperature for L-band radiometry. Inter-comparison and long term validation with SMOSREX field experiment. In: Mätzler, C., Rosenkranz, P. W., Battaglia, A. and Wigneron, J.-P. (Eds.), *Thermal Microwave Radiation - Applications for Remote Sensing Electromagnetic Waves Series*. London, UK: IEEE, pp. 312–324.

Dobson, M. C., Ulaby, F. T., Hallikainen, M. T. and El-Rayes, M. A. (1985). Microwave dielectric behavior of wet soil-Part II: Dielectric mixing models. *IEEE Transactions on Geoscience and Remote Sensing* GE–23(1), 35–46.

Dorigo, W., Himmelbauer, I., Aberer, D., Schremmer, L., Petrakovic, I., Zappa, L., Preimesberger, W., Xaver, A., Annor, F., Ardö, J., Baldocchi, D., Bitelli, M., Blöschl, G., Bogena, H., Brocca, L., Calvet, J., Camarero, J. J., Capello, G., Choi, M., Cosh, M. C., van de Giesen, N., Hajdu, I., Ikonen, J., Jensen, K. H., Kanniah, K. D., de Kat, I., Kirchengast, G., Kumar Rai, P., Kyrouac, J., Larson, K., Liu, S., Loew, A., Moghaddam, M., Martínez Fernández, J., Mattar Bader, C., Morbidelli, R., Musial, J. P., Osenga, E., Palecki, M. A., Pellarin, T., Petropoulos, G. P., Pfeil, I., Powers, J., Robock, A., Rüdiger, C., Rummel, U., Strobel, M., Su, Z., Sullivan, R., Tagesson, T., Varlagin, A., Vreugdenhil, M., Walker, J., Wen, J., Wenger, F., Wigneron, J. P., Woods, M., Yang, K., Zeng, Y., Zhang, X., Zreda, M., Dietrich, S., Gruber, A., van Oevelen, P., Wagner, W., Scipal, K., Drusch, M. and Sabia, R. (2021). The international soil moisture network: Serving earth system science for over a decade. *Hydrology and Earth System Sciences* 25(11), 5749–5804.

Du, L., Tian, Q., Yu, T., Meng, Q., Jancso, T., Udvardy, P. and Huang, Y. (2013). A comprehensive drought monitoring method integrating MODIS and TRMM data. *International Journal of Applied Earth Observation and Geoinformation* 23, 245–253.

Dubois, P. C. and Van Zyl, J. (1994). *An Empirical Soil Moisture Estimation Algorithm Using Imaging Radar*. New York: IEEE, vol. 1573, pp. 1573–1575.

Dubois, P. C., Van Zyl, J. and Engman, T. (1995). Measuring soil moisture with imaging radars. *IEEE Transactions on Geoscience and Remote Sensing* 33(4), 915–926.

Engman, E. T. (1990). Progress in microwave remote sensing of soil moisture. *Canadian Journal of Remote Sensing* 16(3), 6–14.

Engman, E. T. and Chauhan, N. (1995). Status of microwave soil moisture measurements with remote sensing. *Remote Sensing of Environment* 51(1), 189–198.

Entekhabi, D., Njoku, E. G., O'Neill, P. E., Kellogg, K. H., Crow, W. T., Edelstein, W. N., Entin, J. K., Goodman, S. D., Jackson, T. J., Johnson, J., Kimball, J., Piepmeier, J. R., Koster, R. D., Martin, N., McDonald, K. C., Moghaddam, M., Moran, S., Reichle, R., Shi, J. C., Spencer, M. W., Thurman, S. W., Tsang, L. and Van Zyl, J. (2010). The soil moisture active passive (SMAP) mission. *Proceedings of the IEEE* 98(5), 704–716.

Escorihuela, M. J., Kerr, Y. H., de Rosnay, P., Wigneron, J.-P., Calvet, J.-C. and Lemaître, F. (2007). A simple model of the bare soil microwave emission at L-band. *IEEE Transactions on Geoscience and Remote Sensing* 45(7), 1978–1987.

Fung, A. K. (1994a). *Microwave Scattering and Emission Models and Their Applications*. Norwood, MA: Artech House.

Fung, A. K. (1994b). *Microwave Scattering, Emission Model and Its Application*. Norwood, MA: Artech House.

Fung, A. K., Li, Z. and Chen, K. S. (1992). Backscattering from a randomly rough dielectric surface. *IEEE Transactions on Geoscience and Remote Sensing* 30(2), 356–369.

Gao, Y., Walker, J. P., Allahmoradi, M., Monerris, A., Ryu, D. and Jackson, T. J. (2015). Optical sensing of vegetation water content: A synthesis study. *IEEE Journal of Selected Topics in Applied Earth Observations and Remote Sensing* 8(4), 1456–1464.

Gao, Z., Xu, X., Wang, J., Yang, H., Huang, W. and Feng, H. (2013). A method of estimating soil moisture based on the linear decomposition of mixture pixels. *Mathematical and Computer Modelling* 58(3–4), 606–613.

Gerhards, M., Schlerf, M., Rascher, U., Udelhoven, T., Juszczak, R., Alberti, G., Miglietta, F. and Inoue, Y. (2018). Analysis of airborne optical and thermal imagery for detection of water stress symptoms. *Remote Sensing* 10(7), 1139.

Grant, J. P., Saleh-Contell, K., Wigneron, J.-P., Guglielmetti, M., Kerr, Y. H., Schwank, M., Skou, N. and Van de Griend, A. A. (2008). Calibration of the L-MEB model over a coniferous and a deciduous forest. *IEEE Transactions on Geoscience and Remote Sensing* 46(3), 808–818.

Hajnsek, I., Jagdhuber, T., Schön, H. and Papathanassiou, K. P. (2009). Potential of estimating soil moisture under vegetation cover by means of PolSAR. *IEEE Transactions on Geoscience and Remote Sensing* 47(2), 442–454.

Hallikainen, M. T., Ulaby, F. T., Dobson, M. C., El-Rayes, M. A. and Wu, L. K. (1985). Microwave dielectric behavior of wet soil-part 1: Empirical models and experimental observations. *IEEE Transactions on Geoscience and Remote Sensing* GE–23(1), 25–34.

Hassan-Esfahani, L., Torres-Rua, A., Ticlavilca, A. M., Jensen, A. and McKee, M. (2014). Topsoil moisture estimation for precision agriculture using unmmaned aerial vehicle multispectral imagery. In: *IEEE International Geoscience and Remote Sensing Symposium (IGARSS)*. New York: IEEE Publications, vol. 2014, pp. 3263–3266.

Helman, D., Bahat, I., Netzer, Y., Ben-Gal, A., Alchanatis, V., Peeters, A. and Cohen, Y. (2018). Using time series of high-resolution planet satellite images to monitor grapevine stem water potential in commercial vineyards. *Remote Sensing* 10(10), 1615.

Hoffmann, H., Jensen, R., Thomsen, A., Nieto, H., Rasmussen, J. and Friborg, T. (2016). Crop water stress maps for an entire growing season from visible and thermal UAV imagery. *Biogeosciences* 13(24), 6545–6563.

Hornbuckle, B. K. and England, A. W. (2005). Diurnal variation of vertical temperature gradients within a field of maize: Implications for satellite microwave radiometry. *IEEE Geoscience and Remote Sensing Letters* 2(1), 74–77.

Hornbuckle, B. K., England, A. W., De Roo, R. D., Fischman, M. A. and Boprie, D. L. (2003). Vegetation canopy anisotropy at 1.4 GHz. *IEEE Transactions on Geoscience and Remote Sensing* 41(10), 2211–2223.

Houtz, D., Naderpour, R. and Schwank, M. (2020). Portable L-band radiometer (PoLRa): Design and characterization. *Remote Sensing* 12(17), 2780.

Jackson, T. J., Hsu, A. Y., Van de Griend, A. and Eagleman, J. R. (2004). Skylab L-band microwave radiometer observations of soil moisture revisited. *International Journal of Remote Sensing* 25(13), 2585–2606.

Jackson, T. J. and Le Vine, D. E. (1996). Mapping surface soil moisture using an aircraft-based passive microwave instrument: Algorithm and example. *Journal of Hydrology* 184(1–2), 85–99.

Jackson, T. J. and O'Neill, P. E. (1987). Salinity effects on the microwave emission of soils. *IEEE Transactions on Geoscience and Remote Sensing* GE–25(2), 214–220.

Jackson, T. J. and Schmugge, T. J. (1989). Passive microwave remote sensing system for soil moisture: Some supporting research. *IEEE Transactions on Geoscience and Remote Sensing* 27(2), 225–235.

Jackson, T. J. and Schmugge, T. J. (1991). Vegetation effects on the microwave emission of soils. *Remote Sensing of Environment* 36(3), 203–212.

Jackson, T. J., Schmugge, T. J. and Wang, J. R. (1982). Passive microwave sensing of soil moisture under vegetation canopies. *Water Resources Research* 18(4), 1137–1142.

Jagdhuber, T., Hajnsek, I., Bronstert, A. and Papathanassiou, K. P. (2013). Soil moisture estimation under low vegetation cover using a multi-angular polarimetric decomposition. *IEEE Transactions on Geoscience and Remote Sensing* 51(4), 2201–2215.

Jonard, F., Weihermuller, L., Jadoon, K. Z., Schwank, M., Vereecken, H. and Lambot, S. (2011). Mapping field-scale soil moisture with L-band radiometer and ground-penetrating radar over bare soil. *IEEE Transactions on Geoscience and Remote Sensing* 49(8), 2863–2875.

Kankaku, Y., Sagisaka, M. and Suzuki, S. (2014). PALSAR-2 launch and early orbit status. In: *IEEE International Geoscience and Remote Sensing Symposium (IGARSS)*. New York: IEEE Publications, vol. 2014, pp. 3410–3412.

Kerr, Y. H., Waldteufel, P., Wigneron, J.-P., Delwart, S., Cabot, F., Boutin, J., Escorihuela, M. J., Font, J., Reul, N., Gruhier, C., Juglea, S. E., Drinkwater, M. R., Hahne, A., Martín-Neira, M. and Mecklenburg, S. (2010). The SMOS mission: New tool for monitoring key elements of the global water cycle. *Proceedings of the IEEE* 98(5), 666–687.

Khan, N. M., Rastoskuev, V. V., Sato, Y. and Shiozawa, S. (2005). Assessment of hydrosaline land degradation by using a simple approach of remote sensing indicators. *Agricultural Water Management* 77(1–3), 96–109.

Kim, S.-B., Tsang, L., Johnson, J. T., Huang, S., Van Zyl, J. J. and Njoku, E. G. (2012). Soil moisture retrieval using time-series radar observations over bare surfaces. *IEEE Transactions on Geoscience and Remote Sensing* 50(5), 1853–1863.

Kirdiashev, K. P., Chukhlantsev, A. A. and Shutko, A. M. (1979). Microwave radiation of the earth's surface in the presence of vegetation cover. *Radiotekhnika i Elektronika* 24, 256–264.

Kite, G. W. and Pietroniro, A. (1996). Remote sensing applications in hydrological modelling. *Hydrological Sciences Journal* 41(4), 563–591.

Lasne, Y., Paillou, P., Freeman, A., Farr, T., McDonald, K. C., Ruffie, G., Malezieux, J.-M., Chapman, B. and Demontoux, F. (2008). Effect of salinity on the dielectric properties of geological materials: Implication for soil moisture detection by means of radar remote sensing. *IEEE Transactions on Geoscience and Remote Sensing* 46(6), 1674–1688.

Laymon, C. A., Crosson, W. L., Jackson, T. J., Manu, A. and Tsegaye, T. D. (2001). Ground-based passive microwave remote sensing observations of soil moisture at S-band and L-band with insight into measurement accuracy. *IEEE Transactions on Geoscience and Remote Sensing* 39(9), 1844–1858.

Le Toan, T., Quegan, S., Davidson, M. W. J., Balzter, H., Paillou, P., Papathanassiou, K., Plummer, S., Rocca, F., Saatchi, S., Shugart, H. and Ulander, L. (2011). The BIOMASS mission: Mapping global forest biomass to better understand the terrestrial carbon cycle. *Remote Sensing of Environment* 115(11), 2850–2860.

Lievens, H., Verhoest, N., De Keyser, E., Vernieuwe, H., Matgen, P., Álvarez-Mozos, J. and De Baets, B. (2011). Effective roughness modelling as a tool for soil moisture retrieval from C-and L-band SAR. *Hydrology and Earth System Sciences Discussions* 7, 4995–5031.

Liu, H.-J., Zhang, Y.-Z., Zhang, X.-L., Zhang, B., Song, K.-S., Wang, Z.-M. and Tang, N. (2009). Quantitative analysis of moisture effect on black soil reflectance. *Pedosphere* 19(4), 532–540.

Liu, W., Baret, F., Gu, X., Tong, Q., Zheng, L. and Zhang, B. (2002). Relating soil surface moisture to reflectance. *Remote Sensing of Environment*, 81(2–3), 238-–246.

Lu, F., Sun, Y. and Hou, F. (2020). Using UAV visible images to estimate the soil moisture of steppe. *Water* 12(9), 2334.

Martinez-Agirre, A., Álvarez-Mozos, J., Lievens, H. and Verhoest, N. E. C. (2017). Influence of surface roughness measurement scale on radar backscattering in different agricultural soils. *IEEE Transactions on Geoscience and Remote Sensing* 55(10), 5925–5936.

Martinez-Vazquez, A., Camps, A., Lopez-Sanchez, J. M., Vall-Llossera, M. and Monerris, A. (2009). Numerical simulation of the full-polarimetric emissivity of vines and comparison with experimental data. *Remote Sensing* 1(3), 300–317.

Mätzler, C., Rosenkranz, P. W., Battaglia, A. and Wigneron, J.-P. (2006). *Thermal Microwave Radiation: Applications for Remote Sensing Electromagnetic Waves Series*. London, UK: IET.

Meesters, A. G. C. A., De Jeu, R. A. M. and Owe, M. (2005). Analytical derivation of the vegetation optical depth from the microwave polarization difference index. *IEEE Geoscience and Remote Sensing Letters* 2(2), 121–123.

Merlin, O., Walker, J. P., Kalma, J. D., Kim, E. J., Hacker, J., Panciera, R., Young, R., Summerell, G., Hornbuckle, J., Hafeez, M. and Jackson, T. (2008). The NAFE'06 data set: Towards

soil moisture retrieval at intermediate resolution. *Advances in Water Resources* 31(11), 1444–1455.

Merlin, O., Walker, J. P., Panciera, R., Young, R., Kalma, J. D. and Kim, E. J. (2007). Calibration of a soil moisture sensor in heterogeneous terrain with the national airborne field experiment (NAFE) data. In: Oxley, L. and Kulasiri, D. (Eds.), *MODSIM 2007 International Congress on Modelling and Simulation*. New Zealand: Modelling and Simulation Society of Australia, pp. 2604–2610.

Metternicht, G. and Zinck, J. A. (2008). *Spectral Behavior of Salt Types*. Boca Raton, FL: CRC Press.

Metternicht, G. I. and Zinck, J. A. (2003). Remote sensing of soil salinity: Potentials and constraints. *Remote Sensing of Environment* 85(1), 1–20.

Mironov, V. L., Dobson, M. C., Kaupp, V. H., Komarov, S. A. and Kleshchenko, V. N. (2004). Generalized refractive mixing dielectric model for moist soils. *IEEE Transactions on Geoscience and Remote Sensing* 42(4), 773–785.

Mo, T., Choudhury, B. J., Schmugge, T. J., Wang, J. R. and Jackson, T. J. (1982). A model for microwave emission from vegetation-covered fields. *Journal of Geophysical Research* 87(C13), 11229–11211,11237.

Mo, T. and Schmugge, T. J. (1987). A parameterization of the effect of surface roughness on microwave emission. *IEEE Transactions on Geoscience and Remote Sensing* GE–25(4), 481–486.

Monsivais-Huertero, A., Liu, P.-W. and Judge, J. (2018). Phenology-based backscattering model for corn at L-band. *IEEE Transactions on Geoscience and Remote Sensing* 56, 4989–5005.

Newton, R. and Rouse Jr., J. (1980). Microwave radiometer measurements of soil moisture content. *IEEE Transactions on Antennas and Propagation* 28(5), 680–686.

Njoku, E. G. and Entekhabi, D. (1996). Passive microwave remote sensing of soil moisture. *Journal of Hydrology* 184(1–2), 101–129.

Njoku, E. G., Jackson, T. J., Lakshmi, V., Chan, T. K. and Nghiem, S. V. (2003). Soil moisture retrieval from AMSR-E. *IEEE Transactions on Geoscience and Remote Sensing* 41(2), 215–229.

Njoku, E. G. and Kong, J. A. (1977). Theory for passive microwave remote sensing of near-surface soil moisture. *Journal of Geophysical Research* 82(20), 3108–3118.

Njoku, E. G., Wilson, W. J., Yueh, S. H., Dinardo, S. J., Li, F. K., Jackson, T. J., Lakshmi, V. and Bolten, J. (2002). Observations of soil moisture using a passive and active low-frequency microwave airborne sensor during SGP99. *IEEE Transactions on Geoscience and Remote Sensing* 40(12), 2659–2673.

Notarnicola, C., Angiulli, M. and Posa, F. (2008). Soil moisture retrieval from remotely sensed data: Neural network approach versus Bayesian method. *IEEE Transactions on Geoscience and Remote Sensing* 46(2), 547–557.

Oh, Y., Sarabandi, K. and Ulaby, F. T. (1992). An empirical model and an inversion technique for radar scattering from bare soil surfaces. *IEEE Transactions on Geoscience and Remote Sensing* 30(2), 370–381.

Oh, Y., Sarabandi, K. and Ulaby, F. T. (1994). *An Inversion Algorithm for Retrieving Soil Moisture and Surface Roughness From Polarimetric Radar Observation*. New York: IEEE Publications, pp. 1582–1584).

Owe, M., de Jeu, R. and Walker, J. P. (2001). A methodology for surface soil moisture and vegetation optical depth retrieval using the microwave polarization difference index. *IEEE Transactions on Geoscience and Remote Sensing* 39(8), 1643–1654.

Paloscia, S., Pampaloni, P., Chiarantini, L., Coppo, P., Gagliani, S. and Luzi, G. (1993). Multifrequency passive microwave remote sensing of soil moisture and roughness. *International Journal of Remote Sensing* 14(3), 467–483.

Panciera, R., Merlin, O., Young, R. and Walker, J. (2006). *The Hydraprobe Data Acquisition System (HDAS): User Guide*. Report. University of Melbourne.

Panciera, R., Walker, J. P., Jackson, T. J., Gray, D. A., Tanase, M. A., Ryu, D., Monerris, A., Yardley, H., Rudiger, C., Wu, X., Gao, Y. and Hacker, J. M. (2014). The soil moisture active passive experiments (SMAPEx): Towards soil moisture retrieval from the SMAP mission. *IEEE Transactions on Geoscience and Remote Sensing* 52(1), 490–507.

Panciera, R., Walker, J. P., Kalma, J. D., Kim, E. J., Hacker, J. M., Merlin, O., Berger, M. and Skou, N. (2008). The NAFE'05/CoSMOS data set: Toward SMOS soil moisture retrieval, downscaling, and assimilation. *IEEE Transactions on Geoscience and Remote Sensing* 46(3), 736–745.

Panciera, R., Walker, J. P., Kalma, J. D., Kim, E. J., Saleh, K. and Wigneron, J.-P. (2009). Evaluation of the SMOS L-MEB passive microwave soil moisture retrieval algorithm. *Remote Sensing of Environment* 113(2), 435–444.

Peischl, S., Walker, J. P., Rüdiger, C., Ye, N., Kerr, Y. H., Kim, E., Bandara, R. and Allahmoradi, M. (2012). The AACES field experiments: SMOS calibration and validation across the Murrumbidgee River catchment. *Hydrology and Earth System Sciences* 9, 2763–2795.

Periasamy, S. and Ravi, K. P. (2020). A novel approach to quantify soil salinity by simulating the dielectric loss of SAR in three-dimensional density space. *Remote Sensing of Environment* 251, 112059.

Petropoulos, G. P., Ireland, G. and Barrett, B. (2015). Surface soil moisture retrievals from remote sensing: Current status, products & future trends. *Physics and Chemistry of the Earth, Parts A/B/C* 83–84, 36–56.

Rice, S. O. (1951). Reflection of electromagnetic waves from slightly rough surfaces. *Communications on Pure and Applied Mathematics* 4(2–3), 351–378.

Rodriguez-Fernandez, N. J., Aires, F., Richaume, P., Kerr, Y. H., Prigent, C., Kolassa, J., Cabot, F., Jimenez, C., Mahmoodi, A. and Drusch, M. (2015). Soil moisture retrieval using neural networks: Application to SMOS. *IEEE Transactions on Geoscience and Remote Sensing* 53(11), 5991–6007.

Rodríguez-Fernández, N. J., de Souza, V., Kerr, Y. H., Richaume, P. and Al Bitar, A. (2017). Soil moisture retrieval using SMOS brightness temperatures and a neural network trained on in situ measurements. In: Bitar, A. (Ed.), *IEEE International Geoscience and Remote Sensing Symposium (IGARSS)*. New York: IEEE Publications, vol. 2017, pp. 1574–1577.

Rosen, P., Hensley, S., Shaffer, S., Edelstein, W., Kim, Y., Kumar, R., Misra, T., Bhan, R. and Sagi, R. (2017). The NASA-ISRO SAR (NISAR) mission dual-band radar instrument preliminary design. In: *IEEE International Geoscience and Remote Sensing Symposium (IGARSS)*. New York: IEEE Publications, vol. 2017, pp. 3832–3835.

Santi, E., Paloscia, S., Pettinato, S. and Fontanelli, G. (2016). Application of artificial neural networks for the soil moisture retrieval from active and passive microwave spaceborne sensors. *International Journal of Applied Earth Observation and Geoinformation* 48, 61–73.

Schmugge, T., O'Neill, P. E. and Wang, J. R. (1986). Passive microwave soil moisture research. *IEEE Transactions on Geoscience and Remote Sensing* GE-24(1), 12–22.

Schwank, M. and Mätzler, C. (2006). Air-to-soil transition model. In: Mätzler, C., Rosenkranz, P. W., Battaglia, A. and Wigneron, J.-P. (Eds.), *Thermal Microwave Radiation-Applications for Remote Sensing Electromagnetic Waves Series*. London, UK: IEEE, pp. 287–301.

Schwank, M., Wiesmann, A., Werner, C., Mätzler, C., Weber, D., Murk, A., Völksch, I. and Wegmüller, U. (2010). ELBARA II, an L-band radiometer system for soil moisture research. *Sensors* 10(1), 584–612.

Shen, X., Walker, J. P., Ye, N., Wu, X., Boopathi, N., Yeo, I.-Y., Zhang, L. and Zhu, L. (2020). Soil moisture retrieval depth of P-and L-band radiometry: Predictions and observations. *IEEE Transactions on Geoscience and Remote Sensing* 59, 6814–6822.

Shi, J., Chen, K. S., Li, Q., Jackson, T. J., O'Neill, P. E. and Tsang, L. (2002). A parameterized surface reflectivity model and estimation of bare-surface soil moisture with L-band radiometer. *IEEE Transactions on Geoscience and Remote Sensing* 40(12), 2674–2686.

Shi, J., Jiang, L., Zhang, L., Chen, K., Wigneron, J.-P. and Chanzy, A. (2005). A parameterized multifrequency-polarization surface emission model. *IEEE Transactions on Geoscience and Remote Sensing* 43(12), 2831–2841.

Shi, J., Wang, J., Hsu, A., O'Neili, P. and Engman, E. T. (1995). Estimation of soil moisture and surface roughness parameters using L-band SAR measurements. *Proceeding of IEEE Transaction on Geosicence and Remote Sensing* 501, 507–509.

Shoshany, M., Svoray, T., Curran, P. J., Foody, G. M. and Perevolotsky, A. (2000). The relationship between ERS-2 SAR backscatter and soil moisture: Generalization from a humid to semi-arid transect. *International Journal of Remote Sensing* 21(11), 2337–2343.

Shutko, A. M. and Reutov, E. M. (1982). Mixture formulas applied in estimation of dielectric and radiative characteristics of soils and grounds at microwave frequencies. *IEEE Transactions on Geoscience and Remote Sensing* 1, 29–32.

Sidike, A., Zhao, S. and Wen, Y. (2014). Estimating soil salinity in Pingluo County of China using QuickBird data and soil reflectance spectra. *International Journal of Applied Earth Observation and Geoinformation* 26, 156–175.

Singh, R. and Srivastav, S. (1990). Mapping of waterlogged and salt-affected soils using microwave radiometers. *Remote Sensing* 11, 1879–1887.

Smith, A. B., Walker, J. P., Western, A. W., Young, R. I., Ellett, K. M., Pipunic, R. C., Grayson, R. B., Siriwardena, L., Chiew, F. H. S. and Richter, H. (2012). The Murrumbidgee soil moisture monitoring network data set. *Water Resources Research* 48(7), 1–6. doi:10.1029/2012WR011976.

Taghadosi, M. M., Hasanlou, M. and Eftekhari, K. (2019). Soil salinity mapping using dual-polarized SAR Sentinel-1 imagery. *International Journal of Remote Sensing* 40(1), 237–252.

Torres, R., Snoeij, P., Geudtner, D., Bibby, D., Davidson, M., Attema, E., Potin, P., Rommen, B., Floury, N., Brown, M., Traver, I. N., Deghaye, P., Duesmann, B., Rosich, B., Miranda, N., Bruno, C., L'Abbate, M., Croci, R., Pietropaolo, A., Huchler, M. and Rostan, F. (2012). GMES Sentinel-1 mission. *Remote Sensing of Environment* 120, 9–24.

Turner, D., Lucieer, A. and Watson, C. (2011). Development of an unmanned aerial vehicle (UAV) for hyper resolution vineyard mapping based on visible, multispectral, and thermal imagery. In: *Proceedings of the 34th International Symposium on Remote Sensing of Environment*, p. 4.

Ulaby, F. T., Dubois, P. C. and Van Zyl, J. (1996). Radar mapping of surface soil moisture. *Journal of Hydrology* 184(1–2), 57–84.

Ulaby, F. T., Long, D. G., Blackwell, W. J., Elachi, C., Fung, A. K., Ruf, C., Sarabandi, K., Zebker, H. A. and Van Zyl, J. (2014). *Microwave Radar and Radiometric Remote Sensing*. Ann Arbor: The University of Michigan Press.

Ulaby, F. T., Moore, R. K. and Fung, A. K. (1981). *Microwave Remote Sensing: Active and Passive. Volume I-Microwave Remote Sensing Fundamentals and Radiometry*. Boston, MA: Artech House.

Ulaby, F. T., Moore, R. K. and Fung, A. K. (1982). *Microwave Remote Sensing: Active and Passive. Volume II-Radar Remote Sensing and Surface Scattering and Emission Theory*. Boston, MA: Artech House.

Ulaby, F. T., Moore, R. K. and Fung, A. K. (1986). *Microwave Remote Sensing: Active and Passive. Volume III-Volume Scattering and Emission Theory, Advanced Systems and Applications*. Boston, MA: Artech House.

Ulaby, F. T. and Wilson, E. A. (1985). Microwave attenuation properties of vegetation canopies. *IEEE Transactions on Geoscience and Remote Sensing* GE–23(5), 746–753.

Van de Griend, A. A. and Wigneron, J.-P. (2004). The b-factor as a function of frequency and canopy type at H-polarization. *IEEE Transactions on Geoscience and Remote Sensing* 42(4), 786–794.

Van Zyl, J. J., Chapman, B. D., Dubois, P. and Shi, J. (1993). The effect of topography on SAR calibration. *IEEE Transactions on Geoscience and Remote Sensing* 31(5), 1036–1043.

Vergara-Díaz, O., Zaman-Allah, M. A., Masuka, B., Hornero, A., Zarco-Tejada, P., Prasanna, B. M., Cairns, J. E. and Araus, J. L. (2016). A novel remote sensing approach for prediction of maize yield under different conditions of nitrogen fertilization. *Frontiers in Plant Science* 7, 666.

Wagner, W., Lemoine, G., Borgeaud, M. and Rott, H. (1999a). A study of vegetation cover effects on ERS scatterometer data. *IEEE Transactions on Geoscience and Remote Sensing* 37(2), 938–948.

Wagner, W., Lemoine, G. and Rott, H. (1999b). A method for estimating soil moisture from ERS scatterometer and soil data. *Remote Sensing of Environment* 70(2), 191–207.

Walker, J. P., Dumedah, G., Monerris, A., Gao, Y., Rüdiger, C., Wu, X., Panciera, R., Merlin, O., Pipunic, R., Ryu, D. and Zreda, M. (2012). High resolution soil moisture mapping. In: *5th Global Workshop on Digital Soil Mapping*, Sydeny, Australia.

Walker, J. P. and Houser, P. R. (2004). Requirements of a global near-surface soil moisture satellite mission: accuracy, repeat time, and spatial resolution. *Advances in Water Resources* 27, 785–801.

Walker, J. P., Houser, P. R. and Willgoose, G. R. (2004). Active microwave remote sensing for soil moisture measurement: A field evaluation using ERS-2. *Hydrological Processes* 18(11), 1975–1997.

Wang, J., Ding, J., Yu, D., Ma, X., Zhang, Z., Ge, X., Teng, D., Li, X., Liang, J., Lizaga, I., Chen, X., Yuan, L. and Guo, Y. (2019). Capability of Sentinel-2 MSI data for monitoring and mapping of soil salinity in dry and wet seasons in the Ebinur Lake region, Xinjiang, China. *Geoderma* 353, 172–187.

Wang, J. R. (1983). Passive microwave sensing of soil moisture content: The effects of soil bulk density and surface roughness. *Remote Sensing of Environment* 13(4), 329–344.

Wang, J. R. and Choudhury, B. J. (1981). Remote sensing of soil moisture content, over bare field at 1.4 GHz frequency. *Journal of Geophysical Research* 86(C6), 5277–5282.

Wang, J. R., O'Neill, P. E., Jackson, T. J. and Engman, E. T. (1983). Multifrequency measurements of the effects of soil moisture, soil texture, and surface roughness. *IEEE Transactions on Geoscience and Remote Sensing* GE–21(1), 44–51.

Wang, J. R. and Schmugge, T. J. (1980). An empirical model for the complex dielectric permittivity of soils as a function of water content. *IEEE Transactions on Geoscience and Remote Sensing* GE–18(4), 288–295.

Wang, L. and Qu, J. J. (2009). Satellite remote sensing applications for surface soil moisture monitoring: A review. *Frontiers of Earth Science in China* 3(2), 237–247.

Wang, S., Li, X., Han, X. and Jin, R. (2011). Estimation of surface soil moisture and roughness from multi-angular ASAR imagery in the Watershed Allied Telemetry Experimental Research (WATER). *Hydrology and Earth System Sciences* 15, 1415–1426.

Wegmuller, U. and Mätzler, C. (1999). Rough bare soil reflectivity model. *IEEE Transactions on Geoscience and Remote Sensing* 37(3), 1391–1395.

Weidong, L., Baret, F., Xingfa, G., Qingxi, T., Lanfen, Z. and Bing, Z. (2002). Relating soil surface moisture to reflectance. *Remote Sensing of Environment* 81(2–3), 238–246.

Wigneron, J.-P., Chanzy, A., Calvet, J. C. and Bruguier, N. (1995). A simple algorithm to retrieve soil moisture and vegetation biomass using passive microwave measurements over crop fields. *Remote Sensing of Environment* 51(3), 331–341.

Wigneron, J.-P., Kerr, Y. H., Waldteufel, P., Saleh, K., Escorihuela, M.-J., Richaume, P., Ferrazzoli, P., De Rosnay, P., Gurney, R., Calvet, J.-C., Grant, J. P., Guglielmetti, M., Hornbuckle, B., Mätzler, C., Pellarin, T. and Schwank, M. (2007). L-band microwave emission of the biosphere (L-MEB) model: Description and calibration against experimental data sets over crop fields. *Remote Sensing of Environment* 107(4), 639–655.

Wigneron, J.-P., Laguerre, L. and Kerr, Y. H. (2001). A simple parameterization of the L-band microwave emission from rough agricultural soils. *IEEE Transactions on Geoscience and Remote Sensing* 39(8), 1697–1707.

Wigneron, J.-P., Pardé, M., Waldteufel, P., Chanzy, A., Kerr, Y., Schmidl, S. and Skou, N. (2004). Characterizing the dependence of vegetation model parameters on crop structure, incidence angle, and polarization at L-band. *IEEE Transactions on Geoscience and Remote Sensing* 42(2), 416–425.

Ye, N., Walker, J. P. and Rüdiger, C. (2015). A cumulative distribution function method for normalizing variable-angle microwave observations. *IEEE Transactions on Geoscience and Remote Sensing* 53(7), 3906–3916.

Ye, N., Walker, J. P., Wu, X., de Jeu, R., Gao, Y., Jackson, T. J., Jonard, F., Kim, E., Merlin, O., Pauwels, V. R. N., Renzullo, L. J., Rudiger, C., Sabaghy, S., von Hebel, C., Yueh, S. H. and Zhu, L. (2021). The soil moisture active passive experiments: Validation of the SMAP products in Australia. *IEEE Transactions on Geoscience and Remote Sensing* 59(4), 2922–2939.

Ye, N., Walker, J. P., Yeo, I.-Y., Jackson, T. J., Kerr, Y., Kim, E., McGrath, A., PopStefanija, I., Goodberlet, M. and Hills, J. (2020). Toward P-band passive microwave sensing of soil moisture. *IEEE Geoscience and Remote Sensing Letters* 18, 504–508.

Yuan, Q., Shen, H., Li, T., Li, Z., Li, S., Jiang, Y., Xu, H., Tan, W., Yang, Q., Wang, J., Gao, J. and Zhang, L. (2020). Deep learning in environmental remote sensing: Achievements and challenges. *Remote Sensing of Environment* 241, 111716.

Zarco-Tejada, P. J., Berni, J. A. J., Suárez, L., Sepulcre-Cantó, G., Morales, F. and Miller, J. R. (2009). Imaging chlorophyll fluorescence with an airborne narrow-band multispectral

camera for vegetation stress detection. *Remote Sensing of Environment* 113(6), 1262–1275.

Zarco-Tejada, P. J., Guillén-Climent, M. L., Hernández-Clemente, R., Catalina, A., González, M. R. and Martín, P. (2013). Estimating leaf carotenoid content in vineyards using high resolution hyperspectral imagery acquired from an unmanned aerial vehicle (UAV). *Agricultural and Forest Meteorology* 171–172, 281–294.

Zhang, H., Han, M., Chávez, J. L. and Lan, Y. (2017). Improvement in estimation of soil water deficit by integrating airborne imagery data into a soil water balance model. *International Journal of Agricultural and Biological Engineering* 10, 37–46.

Zhao, W. and Li, Z.-L. (2013). Sensitivity study of soil moisture on the temporal evolution of surface temperature over bare surfaces. *International Journal of Remote Sensing* 34(9–10), 3314–3331.

Zhu, L., Walker, J. P. and Shen, X. (2020). Stochastic ensemble methods for multi-SAR-mission soil moisture retrieval. *Remote Sensing of Environment* 251, 112099.

Zhu, L., Walker, J. P., Tsang, L., Huang, H., Ye, N. and Rüdiger, C. (2019a). A multi-frequency framework for soil moisture retrieval from time series radar data. *Remote Sensing of Environment* 235, 111433.

Zhu, L., Walker, J. P., Tsang, L., Huang, H., Ye, N. and Rüdiger, C. (2019b). Soil moisture retrieval from time series multi-angular radar data using a dry down constraint. *Remote Sensing of Environment* 231, 111237.

Zhu, L., Walker, J. P., Ye, N. and Rüdiger, C. (2019c). Roughness and vegetation change detection: A pre-processing for soil moisture retrieval from multi-temporal SAR imagery. *Remote Sensing of Environment* 225, 93–106.

Zhu, L., Walker, J. P., Ye, N. and Rudiger, C. (2016). The effect of radar configuration on effective correlation length. In: *2016 International Conference on Electromagnetics in Advanced Applications (ICEAA)*. New York: IEEE Publications, pp. 820–823.